ESCUELA POLITÉCNICA SUPERIOR DE MONDRAGON UNIBERTSITATEA
MONDRAGON UNIBERTSITATEKO GOI ESKOLA POLITEKNIKOA
MONDRAGON UNIVERSITY FACULTY OF ENGINEERING

Trabajo fin de máster presentado para la obtención del título de
Titulua eskuratzeko master bukaerako lana
Final degree project for taking the degree of

MÁSTER UNIVERSITARIO EN INGENIERÍA INDUSTRIAL
INDUSTRIA INGENIARITZAKO UNIBERTSITATE MASTERRA
UNIVERSITY MASTER IN INDUSTRIAL ENGINEERING

Título del Trabajo *Lanaren izenburua* Project Topic

THERMO-MECHANICAL ANALYSIS OF POWDER BED FUSION PROCESSES

Autor *Egilea* Author ADRIAN ALAMO GUTIERREZ

Curso *Ikasturtea* Year 2020/2021

Título del Trabajo *Lanaren izenburua* Project Topic

THERMO-MECHANICAL ANALYSIS OF POWDER BED FUSION PROCESSES

Nombre y apellidos del autor
Egilearen izen-abizenak
Author's name and surnames
ALAMO GUTIERREZ, ADRIAN

Nombre y apellidos del/los director/es del trabajo
Zuzendariaren/zuzendarien izen-abizenak
Project director's name and surnames
DIOGO MARIANO SIMOES NETO
MENDIGUREN, JOSEBA

Lugar donde se realiza el trabajo
Lana egin deneko lekua
Company where the project is being developed
Universidade de Coimbra

Curso académico
Ikasturtea
Academic year
2020/2021

ABSTRACT

This document includes an end-of-master project carried out by Adrián Álamo Gutíerrez in the University of Coimbra with the aim of completing the studies of the master's in industrial engineering.

Additive Manufacturing (AM) is an attractive technology for producing customized and complex components, in particular the laser powder bed fusion process for metal parts. Nevertheless, the broad range of length- and time-scales associated with the process requires the adoption of multi-scale modelling approaches to obtain predictions at part-scale. This project focuses on the research on the numerical modelling of the Selective Laser Melting (SLM) process. In order to reduce the computational cost of the numerical simulations, in this study the prediction of the residual stresses and part distortion is conducted at meso-scale using the finite element method. The thermomechanical analysis of the SLM process uses volumetric moving heat source. The mechanical analysis is based in a elastoplastic constitutive law, which predicts the residual stresses through the strains induced by the thermal gradients. Both the thermal and the mechanical material properties are assumed as temperature dependent. The computational cost of the numerical simulations is very high due to the requirements of very small-time steps and very refined meshes. Accordingly, two different types of meshes are adopted in the numerical simulations, namely the classical conforming meshes and, non-conforming meshes. They are compared in terms of computational cost and accuracy is the aim of this study.

The single-layer and single-track example adopted to analyse the SLM process. Finally, the influence of the main process parameters on the resulting residual stresses/distortion is analysed. The prediction of the residual stresses and part distortion is expected, providing the basis for the optimization of powder-based AM processes.

Key words: Additive Manufacturing, Selective Laser Melting, Thermomechanical Analysis, finite element method and residual stresses.

LABURPENA

Dokumentu honek Adrián Álamo Gutíerrezek Coimbrako Unibertsitatean burututako master amaierako proiektua biltzen du, industria ingeniaritzako masterra osatzeko helburuarekin.

Fabrikazio Gehigarria (AM) teknologia erakargarria da osagai konplexu eta pertsonalizatuak ekoizteko, batez ere metalezko piezen hauts bidezko laser bidezko urtze prozesua. Hala ere, prozesuarekin lotutako luzera eta denbora eskala sorta zabalak eskala anitzeko modelatze planteamenduak hartzea eskatzen du eskala parteko iragarpenak lortzeko. Proiektu hau laser bidezko fusio selektiboaren (SLM) prozesuaren zenbakizko modelizazioaren ikerketan oinarritzen da. Zenbakizko simulazioen kostu konputazionala murrizteko asmoz, ikerketa honetan hondar tentsioen eta piezaren distortsioaren iragarpena meso eskalan egiten da elementu finituen metodoa erabiliz. SLM prozesuaren analisi termomekanikoak mugitzen den bero iturri bolumetrikoa erabiltzen du. Analisi mekanikoa lege eratzaile elastoplastiko batean oinarritzen da, eta horrek hondar-tentsioak iragartzen ditu gradiente termikoek eragindako deformazioen bidez. Materialaren propietate termikoak eta mekanikoak tenperaturaren menpe daudela suposatzen da. Zenbakizko simulazioen kostu konputazionala oso altua da, denbora-urrats oso txikien eta sare oso finduen eskakizunak direla eta. Ondorioz, zenbakizko simulazioetan bi sare mota desberdin hartzen dira, hau da, konformatzen diren sare klasikoak eta konformatzen ez diren sareak. Ikerketa honen helburua konputazio kostuaren eta zehaztasunaren arabera alderatzea da.

SLM prozesua aztertzeko geruza bakarreko eta modu bakarreko adibidea hartzen da. Azkenik, prozesuaren parametro nagusien ondorioz sortzen diren hondar tentsio / distortsioetan duten eragina aztertzen da. Hondar tentsioak eta piezak distortsionatzearen aurreikuspenak hautsetan oinarritutako AM prozesuak optimizatzeko oinarria izango dela espero da.

Hitz gakoak: Fabrikazio Gehigarria, Laser Bidezko Fusio Selektiboa, Analisi Termo mekanikoa, elementu finituen metodoa eta hondar tentsioak.

RESUMEN

Este documento recoge un proyecto de fin de máster realizado por Adrián Álamo Gutíerrez en la Universidad de Coimbra con el objetivo de completar los estudios del máster en ingeniería industrial.

La fabricación aditiva (AM) es una tecnología atractiva para la producción de componentes personalizados y complejos, en particular el proceso de fusión por láser de lecho de polvo para piezas metálicas. Sin embargo, la amplia gama de escalas de longitud y tiempo asociadas al proceso requiere la adopción de enfoques de modelización multi escala para obtener predicciones a escala de pieza. Este proyecto se centra en la investigación de la modelización numérica del proceso de fusión selectiva por láser (SLM). Con el fin de reducir el coste computacional de las simulaciones numéricas, en este estudio la predicción de las tensiones residuales y la distorsión de la pieza se realiza a escala meso utilizando el método de los elementos finitos. El análisis termo mecánico del proceso de SLM utiliza una fuente de calor volumétrica en movimiento. El análisis mecánico se basa en una ley constitutiva elastoplástica, que predice las tensiones residuales a través de las deformaciones inducidas por los gradientes térmicos. Tanto las propiedades térmicas como las mecánicas del material se suponen dependientes de la temperatura. El coste computacional de las simulaciones numéricas es muy elevado debido a los requisitos de pasos de tiempo muy pequeños y mallas muy refinadas. En consecuencia, se adoptan dos tipos diferentes de mallas en las simulaciones numéricas, a saber, las mallas conformes clásicas y las mallas no conformes. Su comparación en términos de coste computacional y precisión es el objetivo de este estudio.

El ejemplo de una sola capa y de una sola vía se adopta para analizar el proceso de SLM. Por último, se analiza la influencia de los principales parámetros del proceso en las tensiones residuales/distorsiones resultantes. Se espera que la predicción de las tensiones residuales y la distorsión de la pieza proporcione la base para la optimización de los procesos de AM basados en polvo.

Palabras clave: Fabricación Aditiva, Fusión Selectiva por Láser, Análisis Termo mecánico, método de elementos finitos y tensiones residuales.

INDEX

FIGURE INDEX

TABLES INDEX

1. INTRODUCTION

The main aim of this introductory section is to describe the project research that is explained in this document, as well as the main objectives and its development phases. During this document, the project developed by Adrian Alamo Gutierrez in University of Coimbra between November of 2020 and July of 2021, for getting the master's degree of Industrial Engineering is described in detail.

1.1. MOTIVATION

This section gives a brief introduction to Additive Manufacturing (AM), which is an emerging manufacturing method where material is added layer-by-layer for creating a physical component from a digital model [1]. This unique feature allows production of complex and customized parts directly from the design without the need for expensive tooling such as punches, dies or casting moulds and reduces the need for many conventional processing steps. The AM processes consolidate feedstock material such as powder, wire or sheets into a dense metallic part by melting and solidification with the aid of an energy source such as lase, electron beam or electric arc, or by the use of ultrasonic vibration in a layer-by-layer manner [2]. This type of technology offers a new fabrication perspective which reduces material waste leading buy-to-fly ratios near to 1. This ratio relates the amount of material needed to buy compared to the amount of material that will end up finally flying.

The AM also enables more design freedom avoiding the need to manufacture difficult clamping tools [3]. Furthermore, parts can be produced on demand, reducing the inventory of spares and decreasing lead time for critical or obsolete replacement components. For this reason, AM is now widely accepted as a new paradigm for the design and production of high-performance components for aerospace, medical, energy and automotive applications [4].

Nevertheless, the as-built surface roughness might not meet the functional requirements. Moreover, the cyclic melting and solidification creates a complex thermal history, which produces high tensile residual stresses and consequent

distortion of the manufactured components. Therefore, the process parameters must be adjusted to minimize the occurrence of such defects. However, the experimental tuning of these process parameters is very expensive and time-consuming since they are intertwined with each other.

Within this frame, it is the opinion of the present authors that the industrial integration of these shaping techniques may be facilitated by the use of numerical simulations of selective laser melting. The numerical simulations may replace (or at least reduce) the tedious trials and errors optimization of digital processing technologies [5].

1.2. ADDITIVE MANUFACTURING

AM is an emerging field, and new production methods and principles are continuously being developed. ASTM has defined seven main categories of AM, these are shown in Figure 1, a short description of the categories follows bellow.

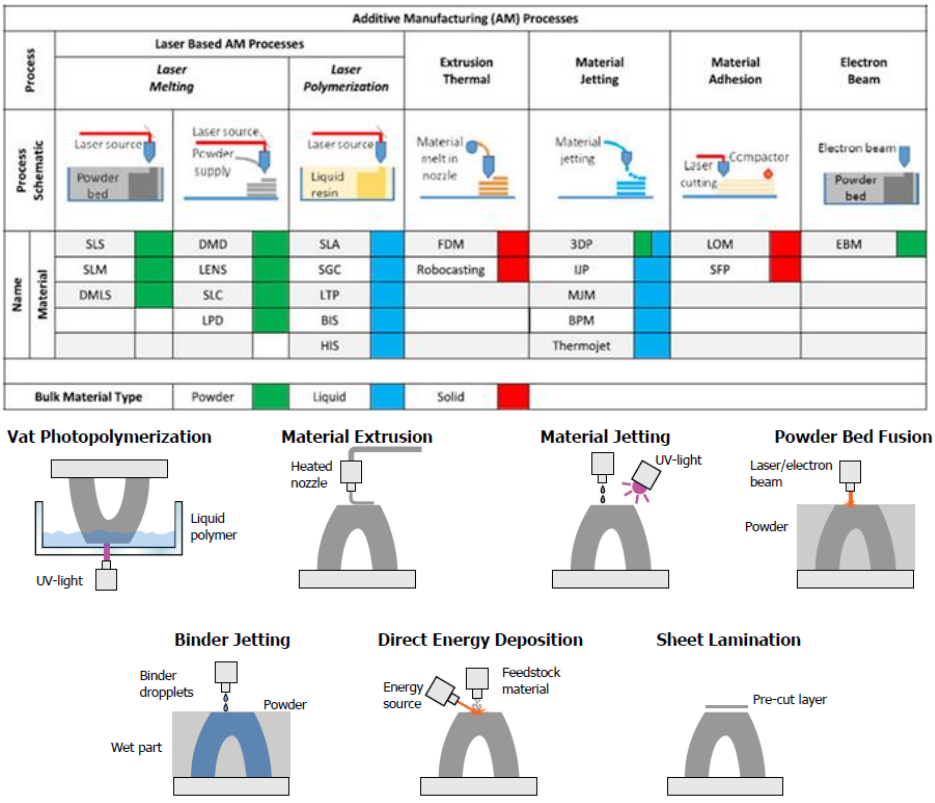

Figure 1*: Processes category for AM technologies* [2].

1.2.1. DIRECT METAL DEPOSITION

Direct metal deposition (DMD) is a group of technologies originating from laser cladding, which involves progressively overlaying deposited weld beads to form a structure. The material deposited may originate from a powder source or solid wire feedstock, which are fused thermally, either using a laser or by electric are. These technologies offer the highest deposition rates and build volume for additive manufactured metal parts, at the expense of resolution [6].

1.2.2. VAT PHOTOPOLYMERSIZATION

Vat photopolymerization is based on curing liquid polymers by the use of a UV light. Usually, a platform is immersed into liquid polymer, then a UV-light selectivity cures the polymer from below. This process is repeated layer by layer until a solid part is formed, afterwards, additional curing may be required for archiving desired properties of the part [1].

1.2.3. MATERIAL EXTRUSION

Material Extrusion is based on extruding material though a heated nozzle. The material is extruded and deposited in a selective manner layer by layer for forming the final component. Typical materials are thermoplastics, but the method can be used for other materials such as concrete [1]. This process is typically used in the personal 3D printings.

1.2.4. MATERIAL JETTING

Material Jetting is one of the fastest and most accurate 3D printing techniques [7]. It is based on jetting material to form a solid. The process is similar to material extrusion, but rather than continuously extruding material, it is jetted onto the part in droplets. After the droplets are jetted onto the part they are cured by a UV-lamp [1].

1.2.5. BINDER JETTING

Binder Jetting is similar to powder bed fusion, but rather than directly fusing together the powder particles, a binder is used to bind the particles together

creating a wet ¨green part". The green part is cured afterwards for removing the binder and fusing together the powder particles [1]. The main advantages of this process lie in its acceptable speeds, the recyclability of un-used material, and the omission of supporting structures. However, the technique does not allow for the fabrication of hollow parts, since an opening must be included to empty the powder in the interior [7].

1.2.6. SHEET LAMINATION

Sheet Lamination process involves the rapid prototyping of objects by stacking layers of materials in form of sheets and adhering these together using a bonding agent. The material feedstock is available in form of a continuous sheet wound around a spool. The sheet is pulled over the building platform and adhered to it using a heated roller. A laser cutter or a knife is used to cur the contour of the cross-section in the given layer. The wasted material (non-part sheet) is collected over a second drum. The platform with the completed layer is then lowered and a new sheet is bonded to the previous layer. These steps are repeated until the prototype is completed [7].

1.2.7. POWDER BED FUISION

Powder Bed Fusion is based on directly fusing together powder particles. Powder is spread in an even layer, and the powder particles are fused together layer by layer by a moving energy source. For metals, a laser or electron beam is usually used [1].

1.2.8. INITIAL COST ESTIMATION

The decision to use AM processes for functional parts involves balancing the cost of AM against the expected benefits during the design, production and use phase. Although the cost/benefits analysis during the early design stage is important, information required for detailed cost estimation is often missing. Knowledge on the expected product volume, production technology and required post-processing steps can give insight into the expected costs. For the early cost estimation on the production of the part, the cost is often expressed as cost per

cm^3 of the printed part. In the study [8] they have been estimated some costs for the materials and the processes and also for the post-processing operations. Table 1 presents the cost per cm^3 of the printed part for different materials and processes, based on the assumption of an optimal utilization of the build envelope. The values presented are only indicative since the calculation method and constants used have a large impact on the price. The typical cost of post-processing operations is presented in Table 2. Post-processing can add considerably to the cost of AM parts. The reasons that post-processing steps have a larger effect on the cost are their labour intensity.

Table 1*: Cost price per cm3 for different materials and processes, based on the assumption of an optimal utilization of the build envelope and in house production. The values presented are indicative only, as the calculation method and constants used have a large impact on the price per cm3 presented* [8]*.*

Process	Material	Post Proc.	€/cm
L-PBF	SS 304L	WE, SR, PR	8.25
	17-4 PH	WE, SR, PR	6.62-8.63
	17-4 PH	WE	7.17
	316L	WE	7.03
	AlSi 10Mg	HT	7.97
	Titanium	Undefined	5.68
E-PBF	Ti-6Al-4V	None	2.77
	Titanium	Undefined	4.54
DED - powder	Titanium	Undefined	2.11
DED - wire	Titanium	Undefined	2.11
Binder Jetting	Titanium	Undefined	1.96

Table 2: *Cost of post-processing operations* [8].

Technique	Improvement goal	Cost indication
Stress relieves	Reduction/removal of thermal residual stresses	$500-600 per build plate
Part Removal	Remove part from the build plate - w - EDM	$200-300 per build plate
	Remove part from the build plate – Band saw	Low cost
Heat treatment	To improve microstructure & mechanical properties	$500 to $2,000 per batch
Hot isostatic pressing	To reduce porosity and improves fatigue live	$500 to $2,000 per batch
Machining	To improve accuracy of mating interfaces and surface. To add threads and remove supports.	Cost depends on geometry & material and fixture needs.
Surface treatments	Improve surface finish/quality/surface roughness	$200 to 2,000 per batch
Inspection & Testing	Process qualification and part validation & certification	10-20% of total cost per part

1.2.9. ENVIROMENTAL IMPACT OF THE AM

Environmental considerations are taking an important place in the manufacturing world. In fact, green manufacturing is defined as the first step towards sustainability development. In the field of machining process with “chip removing,” several works have been carried out considering environmental considerations [9]. Conducting energy consumption and environmental impact analysis for AM processes is a challenging but necessary task. Although environmentally conscious manufacturing has received increasing interest since the 1990s, there is not a uniformly satisfactory quantitative method to evaluate the environmental impacts of manufacturing processes. The environmental analysis for manufacturing processes should include process time, energy utilization, primary flow of work-piece materials, and secondary flows of process catalysts [10].

Based on the theory of industrial ecology, there are two major methods for environmental impact assessment, namely, environmental impact assessment (EIA) and life-cycle analysis (LCA). However, these methods often cannot measure the actual environmental impacts directly, predict effects, or represent causal linkages with specific effects. In addition, weighting factors are normally given in a descriptive language, such as “low,” “moderate,” and “serious” which is difficult if not impossible to transform into numbers and solve mathematically [10].

AM enables environmentally friendly product design. Unlike traditional manufacturing processes that place many constraints on product design, the flexibility of AM allows manufacturers to optimize design for lean production, which by its nature eliminates waste [10]. The impacts of AM and traditional CNC machining can be directly compared in some ways, but not in others. Both use significant amounts of electricity, in both cases, the electricity use is largely time-dependent and is also dependent on part geometry or finish quality, primarily through their effects on processing time. The primary difference between AM and CNC in types of impacts is that machining generally uses cutting oil for lubrication, which is an additional source of waste [11].

The economic advantages of metal AM as alternative to traditional methods are clear, but the reduce environmental impact may be even more important to the future industry. Each of the four environmental drawbacks of convectional manufacturing listed above has the potential to be mitigated by 3D printing [12].

1.2.10. SOCIAL IMPACT

The literature provides some evidence of AM technology's social impacts on work and labour conditions. The apparent "clean" aspect of AM causes little preoccupation about individual safety, caution around the handling and disposal of materials, and consideration of a proper location for the equipment. AM technology can create unemployment and political destabilization in some economies, leading to changes in labour intensity, employment schemes, types of work, work conditions, working hours, working places, and employment policies, or even in changes in labour laws. Conversely, positive impacts are foreseen, such as digipreneurship (digital entrepreneurship), allowing the creation of niche markets, access for people without prior knowledge of design and/or production to create diverse product types, and avoiding the need to go to work to big cities, among other social innovations related to the easy self-use and flexibility of AM technology. The adoption of AM technology is also mentioned as positive to "especially aging societies, (that) might benefit from the ability to produce more goods with fewer people while reducing reliance on imports" [13].

The reduction of health costs for the elderly and the rise of life expectancy and quality AM social impacts, mainly because of the possible customizations of healthcare products (e.g., surgical implants, orthodontics, etc.) [13].

1.3. SELECTIVE LASER MELTING PROCESS

Selective laser melting (SLM) is an AM method contained in the powder bed fusion group. This method allows the production of parts directly from 3D CAD models by the selective fusion of the powder bed. It is made by a repetitive process of deposition and guided laser melting of an atomized metallic particle bed. The laser melts the powder particles, creating a melt pool that penetrates

the previously deposited build layers, joining the two upon cooling. Once complete, the build bed is incrementally lowered one-layer thickness and the process repeated, see Figure 2.

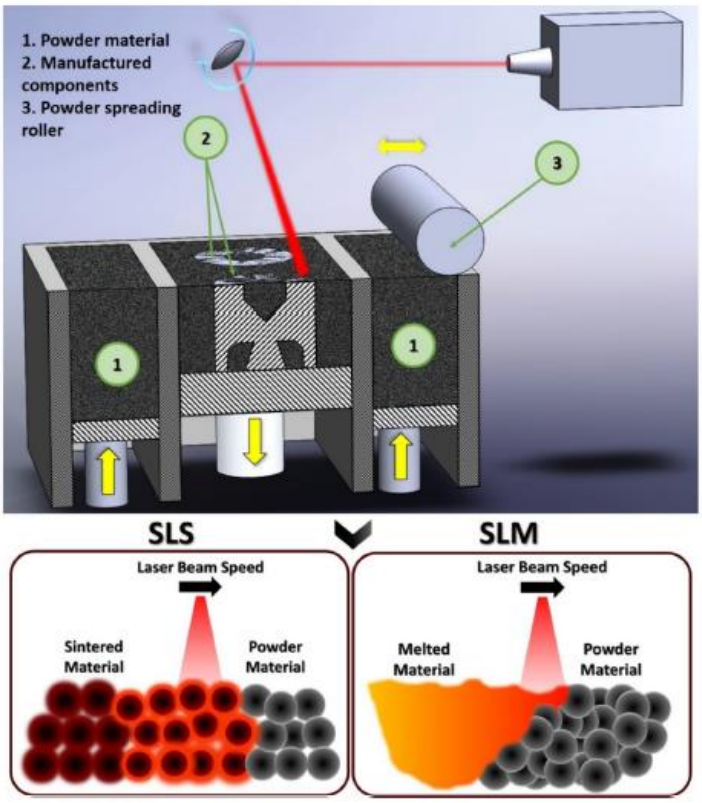

Figure 2: *Selective melting laser process* [14].

SLM process have some disadvantages, which currently require a lengthy process of part qualification and certification to detect flaws including high residual stress, porosity, disconnected layers and undesired micro-structures. One of the most important problems of the SLM process is the high residual stress that can change the mechanical properties or create distortions. To avoid undesirable failures of the component due to the residual stresses and distortions, the usage of support structures is exploited during SLM process, which results in minimizing the residual stresses and distortions of the component. The support structures are made up of the same material of which the component is being made. This support structure offers support to the overhanging part of the built component. The effective design of support structure helps to avoid cracking and distortion [15].

The physical phenomena associated with SLM are highly complex and include scattering and absorption of laser radiation in the packed powder bed, heat conduction, melting and fusion of the powder particles, the formation and solidification of the melt pool. SLM processing parameters fall into four main categories, namely: (1) laser related parameters; (2) scan related parameters; (3) powder related parameters; and (4) temperature related parameters. These parameters are mutually interactive in the manufacturing process and have a profound effect on the mechanical properties of the final component [16]. Consequently, relying on experimental trial-and-error methods to determine the optimal SLM processing conditions is extremely inefficient and time consuming. Thus, simulation models for estimating the suitable parameters are commonly preferred [16]. In order to minimize costly trial and error approach by repeated experiments, numerical simulation has been introduced and continuously developed to model the thermal and mechanical responses during and after processing [17]. In order to improve the process, multiple studies on the manufacturing process, materials, process parameters, etc. must be carried out. For this purpose, finite element simulations are essential and help in the speed and accuracy on the research. A good characterization of the model is necessary to get a low computational cost and accuracy in the results.

For the purpose of reduce the computational cost and have better accuracy the mesh of the simulation is very important. This study will develop how to optimise the mesh to achieve these two purposes. Specifically, this study has focused on the differences between the conforming and the non-conforming mesh.

1.4. NUMERICAL MODELLING

The finite element method is a numerical technique for the approximate solution to a set of continuous partial different equations encountered when modelling physical phenomena [6]. There are several computational methods currently adopted in the numerical simulation of the SLM process. This section described the main computational methods currently adopted in the numerical simulation of the SLM process.

1.4.1. MICRO-SCALE MODELLING

Micro-scale consists of modelling the interactions between the laser and particles at the 'powder scale'. The sintering behaviour and the dynamic formation of the melt pool can be tracked. The models must some degree account for the thermo-fluid physics involved and provide information on the formation and stability of the melt pool along a track or layers. Simulations at the micro-scale are inherently expensive owing to the high resolution required [6].

1.4.1.1. MELT FLOW DYNAMICS

Melt pool dynamics are driven mainly by capillary and Marangoni forces, evaporation pressure, and the wetting ability of the powder particles and the previous layer [18]. One of the major challenges in computational fluid dynamics (CFD) modelling of such processes is the description of surface tension and its local variations with temperature and chemical composition. These variations are at the origin of Marangoni flow within the liquid, which significantly affects the shape and depth of the melt pool. Accurate simulation of the melt pool geometry and the possible gas entrapment at the origin of voids and defects are crucial to the prediction of the final quality of the parts.

1.4.1.2. DISCRETE ELEMENT MODELLING OF POWDER

Apart from the details regarding the modelling of thermal and fluid flow phenomena, residual stresses and microstructure alterations, there are also some other important issues, which should be taken into account for an accurate and realistic simulation of SLM. These issues are relevant to the modelling of the powder, which constitutes the raw material for SLM. More specifically, in simulations of SLM, modelling of the powder layers, as well as the procedure of spreading the powder before it is irradiated by the laser beam, is essential to be conducted in order to achieve higher accuracy of the results and higher degree of realism of the simulation.

The powder can be also modelled by appropriate numerical methods. In most of the studies they consider the powder layer as a continuum domain

although with suitable material properties, in the earliest stages of the additive manufacturing process, the discrete nature of the powder should be taken into consideration. In the later stages of the simulation, the powder domain can be also discretized with finite elements in the same way as the substrate and solved according to the numerical schemes adopted for the FE analysis of the whole computational domain.

However, modelling of powder during its initial deposition and spreading cannot be performed by the FE method due to its discrete nature. Thus, a meshless method, which can account for the interactions between particles of the powder is required to be employed, with the most suitable being the Discrete element method (DEM) [14].

1.4.2. MESO-SCALE

Meso-scale consists of modelling sub-regions of the process, typically several scan vectors over a series of layers. Given the coarser resolution and large timeframe required, the thermo-mechanical behaviour is usually captured, and can predict the residual stress distribution within the zone. The thermal response provides an input to determine the micro-structural evolution of the metallurgy for a built material [6].

1.4.3. MACRO-SCALE

Macro-scale consists of modelling information for large regions or parts. Model abstractions are used to reduce complexity of the underlying physics captured downwards at micro and meso scales [6].

1.5. OBJECTIVES

The main objective of this study is the numerical modelling of the SLM process using the finite element method. In order to reduce the computational cost of the simulations, different approaches are adopted to create the meshes, namely the adoption of conforming and non-conforming meshes. For this purpose, technical objectives have been defined and for each of these objectives specific tasks have been defined:

- Carry out a literature review research in order to introduce to the selective laser melting process.
    - Study of the computational methods currently adopted in the numerical analysis of AM processes.
    - Lis of parameters to take into account to simulate Selective Laser Melting (SLM) processes using the Finite Element Method (FEM).
    - Experimental data currently available to validate the numerical models.
    - Experimental techniques to measure the residual stresses within parts build by metal-based AM.
    - Accuracy of the indirect techniques to evaluate the stress level using the part distortion measurements.
    - Capability of high-speed cameras to measure the melt pool geometry and dimensions.
    - Experimental techniques to measure both thermal and mechanical properties of metallic materials in a wide range of temperatures.
- Analyse the finite element analysis of SLM process, first of all the thermal problem and once that this problem is understood solution of the thermo-mechanical problem.
    - Solution of the transient thermal problem.
    - Solution of the mechanical problem for asses the residual stresses.
- Learn the DD3IMP finite element code and run the simulations with this same code.
    - Main feature and formulation of the software.
    - Relationship between computational cost and accuracy.
    - Thermo-elasto-plastic calculations of the SLM process in different situations and with different process parameters.
- Analyse the results obtained in the simulations.
    - Analise the result obtained 2D.
    - Analise the result obtained 3D.

1.6. SPECIFICATIONS

This project deals with the numerical analysis of the Selective Laser Melting (SLM) processes. Some problems appear in the manufacturing of the AM process. One of the most common failures in the SLM process is caused by the accumulation of stresses that lead to cracks or distortions in the part. A better understanding of SLM is required to minimize these defects and allow for its full adoption by industry. This is the reason why we are going to research SLM process. To this end, a series of phases have been followed:

1. Literature review of the topic, focused on the numerical modelling strategies.
2. Understanding the numerical methods currently implemented in DD3IMP finite element code, namely the a solution of the thermal and mechanical problem.
3. Numerical analysis of the SLM process using the DD3IMP finite element code.
4. Presentation and discussion of the results obtained.

The following standard constrains have been taken into account for the optimization of this project:

- Microsoft Word and Excel have been used for the drafting and creation of tables for this project.
- DD3IMP finite element code has been used for the simulations in 2D and 3D.
- For the pre-processing and post-processing the GID program has been used.
- Internal thesis from the University of Coimbra.

1.7. PROJECT PHASES

- Literature review: The objective of this task is to collect recent studies about the SLM process, namely the numerical modelling of powder based additive manufacturing processes. The exponential

growth of publications about the AM requires a rigorous selection of the references used to support this study.

The core of this task comprises a critical literature review, focused on the computational methods currently available to simulate the SLM process. Different approaches have been developed, aiming the analysis of different process features. The numerical analysis ranges from the modelling of the melt pool dynamics up to the modelling of entire geometry of the workpiece to be built. Nevertheless, since the final objective is the prediction of residual stress and part distortion, the mechanical analysis of the built part is privileged. The interaction and the mapping of the information between different scales is important to predict the residual stresses and part distortion through a multi-scale approach. The advantages and drawbacks of each approach must be highlighted and discussed.

The computational models need to be validated with rigorously controlled experimental results. Therefore, the literature review about the experimental techniques currently adopted to validate the numerical models is also important. Hence, this task includes a depth review of the following topics: (i) experimental techniques to measure the residual stresses within parts built by metal based AM, namely X-ray diffraction measurements; (ii) accuracy of the indirect techniques to evaluate the stress level using the part distortion measurements; (iii) capability of high-speed cameras to measure the melt pool geometry and dimensions; infrared cameras and thermocouples to measure the temperature field and (iv) experimental techniques to measure both thermal and mechanical properties of metallic materials in a wide range of temperatures. The finite element simulations require a wide range of thermo-physical properties of the material, which typically are temperature dependent.

- Study of the numerical methods: The aim of this study is the thermo-mechanical analysis of the SLM process. Therefore, it is essential the study of the main algorithms involved in these simulations. The solution of the transient thermal problem using the finite element method is the first step. The starting point is the differential equation governing the transient heat conduction. The power generated per volume in the workpiece arises in this equation. Different strategies are available to model the heat source. Due to the porosity in the powder bed, the incident laser radiation is reflected between the particles, increasing the absorption depth in comparison to the one observed for the bulk solid. Thus, the laser heat input is modelled by the volumetric Gaussian heat source proposed by Goldak. Thermal convection and radiation boundary conditions are applied on the top layer during the deposition. Typically, the lateral sides of the model are thermally insulated. The integration of the discretized finite element equations for heat transfer problems is carried out using the generalized trapezoidal method. Then, the generalized trapezoidal method can take the form of well-known time integration methods such as, Euler forward method, Crank-Nickolson method, Galerkin method and Euler backward method.

  The numerical prediction of the residual stresses/distortion requires the solution of the mechanical problem (quasi-static analysis). The stresses arise due to the thermal gradients and the thermal expansion of the material. The localized heating leads to a volumetric expansion of the material in that zone, which generates residual stresses and consequently distortions in the final part. Since the magnitude of the residual stresses result can exceed the yield strength of the alloy, modelling the elasto-plastic behavior of the material is required. Moreover, the SLM process includes the transformation of powder particles to molten metal upon beam exposure, and solidification of liquid metal upon cooling. Therefore, any material point in the FE model can take one of the three states of powder, liquid, or solid. The powder/solid elements transform to

the liquid state as the temperature rises above the melting point and upon cooling down below the melting temperature, the liquid changes to solid. The powder bed is considered as a continuum with a certain percentage of porosity. In order to accurately predict the coupling between the transient temperature history and the mechanical response, both the thermal and mechanical material properties are assumed as temperature dependent. The staggered coupling can be used to transfer information between thermal and mechanical problems, where the thermal and the mechanical problems are solved sequentially in each time increment.

- DD3IMP finite element code: The numerical simulations will be carid out using the in-house finite element code DD3IMP, which was originally developed to simulate sheet metal forming processes. The solution of the transient heat conduction problem is obtained using the Euler's backward method, while the evolution of the deformation is described by an updated Lagrangian scheme. Both the thermal and the mechanical problems use the same finite element mesh (linear hexahedral elements). In this study conforming and non-conforming meshes are compared in terms of computational cost and accuracy. In this study, the analysis will be restricted to a single layer.

1.8. GANT DIAGRAM

The tasks carried out with the estimated time in blue and the reality of how the tasks have been carried out in green are represented graphically (Figure 3). The red colour represents the delays in the task.

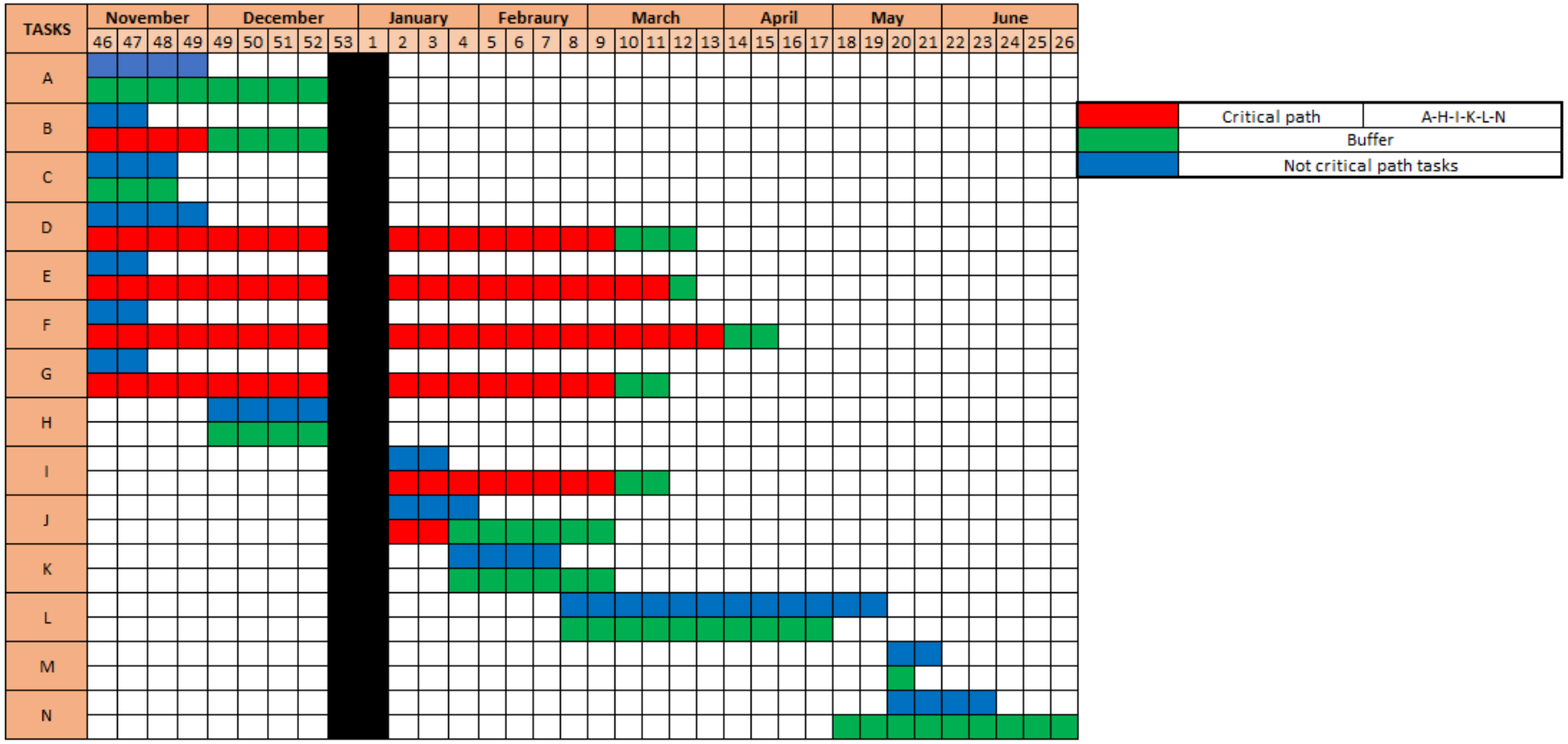

Figure 3: *Gantt diagram project planification.*

2. THERMO MECHANICAL FINITE ELEMENT ANALYSIS

This section presents, the analysis of the transient heat conduction within a solid, the elastoplastic material behaviour under quasi-static loading conditions, as well as the staggered thermo-mechanical coupling. The main objective of this study is the study of non-conforming finite element meshes to reduce the computational time by improving the pre-processing of the simulations. The comparison between conforming and non-conforming meshes is needed in terms of computational cost and accuracy of the numerical solution.

2.1. TRANSIENT HEAT CONDUCTION ANALYSIS

The differential equation of heat conduction, can be derived from the law of conservation of energy (first law of thermodynamic) applied to a continuous medium with arbitrary volume bounded by a closed surface *S.* The solution of the heat equation (Eq. (1)) gives the temperature distribution of the arbitrary volume with respect to time and can be expressed as follows:

$$\rho c \frac{\partial T}{\partial t} + \mathrm{div}(\mathbf{q}_\mathrm{k}) = \dot{q} \tag{1}$$

where ρ and *c* represent the specific mass and the specific heat capacity of the continuous medium, respectively. The vector $\mathbf{q}_\mathrm{k}$ represents the conduction heat flux and $\dot{q}$ is the energy rate generation per unit of volume. The heat conduction flux is defined by the Fourier law of conduction (Eq. (2)), as follows:

$$\mathbf{q}_\mathrm{k} = -\mathbf{k}\,\mathrm{grad}(T) \tag{2}$$

where **k** is the thermal conductivity tensor, which contains the thermal conductivity in each direction. Combining Eq. (1)and (2), the relation governing the heat conduction can be written as:

$$\rho c \frac{\partial T}{\partial t} = \mathrm{div}[\mathbf{k}\mathrm{grad}(T)] + \dot{q} \quad \textbf{(3)}$$

The classical boundary heat exchanges conditions comprise the heat transfer modes of convection and radiation. To model the convection boundary condition, it is necessary to know the convection coefficient h_c and the exterior temperature T_∞ in order to define the convection heat flux as follows:

$$q_{\mathrm{conv}} = h_{\mathrm{c}}(T - T_\infty) \quad \textbf{(4)}$$

The radiation boundary condition term is defined also based on a heat flux:

$$q_{\mathrm{rad}} = h_{\mathrm{r}}(T - T_{\mathrm{sur}}) \quad \textbf{(5)}$$

In which the h_r is defined by:

$$h_{\mathrm{r}} = \varepsilon\sigma(T^2 + T_{\mathrm{sur}}^2)(T + T_{\mathrm{sur}}) \quad \textbf{(6)}$$

where T_{sur} is the surrounding temperature, ε is the emissivity of the surface and σ is the Stefan-Boltzmann constant.

2.1.1. VOLUMETRIC HEAT SOURCE

The heat source represents laser-matter interaction and advective phenomena occurring inside the melt pool. Furthermore, meso-scale models have limited capabilities due to the continuum powder hypothesis. For this reason, heat is usually applied with a predefined volumetric space distribution dependent on the position of the beam spot, on the laser properties, and on the constitutive parameters of the selected material. If a finite element simulation is adopted, the continuous distributed load is converted into an equivalent nodal thermal flux.

An experimental calibration can be performed to adjust the heat source parameters, thus lowering simulation uncertainties. This calibration consists in the micrographic observation of the MZ and the subsequent tuning of the heat source parameters to replicate its size and shape in the thermal simulation.

Welding simulations suggest that the symmetry of the heat source becomes less and less realistic the more phenomena (e.g. advection inside the melt pool and laser absorption occurring both on the powder particles and on the surface of the molten metal) are included in the heat source model.

To overcome these difficulties, and to reproduce the thermal gradient along the moving direction with greater accuracy, Goldak proposed a double ellipsoidal power density distribution for welding simulation (Eq. (7)). One ellipsoidal source is applied in the half-space x ≥ 0, while the other one is applied in the remaining region.

$$q^m = \begin{cases} \dfrac{6\sqrt{3}aP\psi_f}{\pi\sqrt{\pi}r_f r_y r_z} e^{-3\left(\frac{x^2}{r_f^2}+\frac{y^2}{r_y^2}+\frac{z^2}{r_z^2}\right)} & \text{if} \quad x \geq 0 \\ \dfrac{6\sqrt{3}aP\psi_f}{\pi\sqrt{\pi}r_r r_y r_z} e^{-3\left(\frac{x^2}{r_r^2}+\frac{y^2}{r_y^2}+\frac{z^2}{r_z^2}\right)} & \text{if} \quad x < 0 \end{cases} \tag{7}$$

where:

- ψ_f is the power fraction deposited in the half-space $x \geq 0$
- $\psi_f = 2 - \psi_f$ is the power fraction deposited in the half-space $x < 0$
- r_f, r_y, and r_z are the semi-axes of the ellipsoidal frontal isosurface with $q^m = q^m_{max} e^{-3}$
- r_f, r_y, and r_z are the semi-axes of ellipsoidal rear isosurface with $q^m = q^m_{max} e^{-3}$
- P is the laser power and a is the absorptivity.

The continuity of q^m across the plane $x = 0$ (Eq. (8)) is ensured by the following equation:

$$\frac{\psi_{\mathrm{f}}}{r_{\mathrm{f}}} = \frac{\psi_{\mathrm{f}}}{r_{\mathrm{f}}} \tag{8}$$

And by substituting $\psi_f = 2 - \psi_f$, it results in:

$$\psi_{\mathrm{f}} = \frac{2r_{\mathrm{f}}}{r_{\mathrm{f}} + r_{\mathrm{r}}} \tag{9}$$

$$\psi_{\mathrm{f}} = \frac{2r_{r}}{r_{\mathrm{f}} + r_{\mathrm{r}}} \tag{10}$$

Therefore, the unknown parameters are *a,* r_f, r_r, r_y, and r_z.

This solution retains all the advantages of the previously described volumetric heat sources but increases flexibility. For these reasons, it was implemented in many cases for the simulation of AM process [19].

2.1.2. FINITE ELEMENT DISCRATIZATION

Applying the principle of virtual temperatures to the strong form, the general heat equation can be written in the weak form (Eq. (11)) as follows:

$$\begin{aligned}\int_V \delta T pcT dV + \int_V \mathrm{grad}(\delta T) \cdot [\mathbf{k} \cdot \mathrm{grad}(T)] dV \\ + \int_S \delta T h_{\mathrm{conv}} T dS \\ + \int_S \delta T h_r T dS \\ = \int_V \delta T q dV + \int_S \delta T h_{\mathrm{conv}} T_\infty dS + \int_S \delta T h_{\mathrm{r}} T_{\mathrm{sur}} dS.\end{aligned} \tag{11}$$

The weak form is obtained by multiplying the governing Eq. (3) and the convection and radiation boundary conditions (Eqs. (4) and (5)) by an arbitrary virtual temperature distribution δ*T* and integrating over the domains on which they hold. According with this principle, *T* is the solution of the temperature distribution

in the body if and only if Eq. (11) holds for any arbitrary virtual temperature distribution δT that is continuous and satisfies the boundary conditions.

The finite element method involves the division of the volume V under consideration into finite elements. The temperature inside a finite element is interpolated using the shape functions and temperatures at nodes (Eq. (12)), which can be approximated by:

$$\begin{aligned} &\mathbf{T}(x,t)=\mathbf{N}(x)\mathbf{T}(t) && \text{for } V\ \forall t\in]0, t_f], \\ &\mathbf{T}(x,t)=\mathbf{N_s}(x)\mathbf{T}(t) && \text{for } S\ \forall t\in](0, t_f], \end{aligned} \tag{12}$$

Where t_f denotes the final instant of the process. $\mathbf{N}(x)$ and $\mathbf{N}_s(x)$ are matrices containing the shape functions associated with the volume and the surface of the body, respectively. Thus, the discretized finite element equations for heat transfer problems (Eq. (13)) can be written as follows:

$$\mathbf{C}\,\dot{\mathbf{T}} + \left(\mathbf{K}_{\text{cond}} + \mathbf{K}_{\text{conv/rad}}\right)\mathbf{T} = \mathbf{Q} + \mathbf{f} \tag{13}$$

where $\mathbf{C}$ is the thermal capacity matrix and $\mathbf{K}_{\text{cond}}$ and $\mathbf{K}_{\text{conv/rad}}$ are the conductivity and the convection/radiation stiffness matrices, respectively. $\mathbf{Q}$ and $\mathbf{f}$ are the vectors of volumetric heat generation and heat fluxes on the surface, respectively. These matrices and vectors (Eqs. (14), (15), (16) and (17))can be expressed as:

$$\mathbf{C} = \int_V \mathbf{N}^{\mathbf{T}} pc\mathbf{N}dV \tag{14}$$

$$\mathbf{K}_{\text{cond}} = \int_V \mathbf{M}^{\mathbf{T}}\mathbf{k}\mathbf{M}dV \tag{15}$$

$$\mathbf{Q} = \int_V \mathbf{N}^{\mathrm{T}}\dot{q}dV \tag{16}$$

$$\mathbf{f} = \int_S \mathbf{N}_s^{\mathrm{T}} h_{\mathrm{conv}} \mathbf{T}_\infty dS + \int_S \mathbf{N}_s^{\mathrm{T}} h_{\mathrm{r}} \mathbf{T}_{\mathrm{r}} dS \quad \textbf{(17)}$$

where **M**= grad(**N**). The vector of internal heat generation (Eq. ((17)) comprises the heat generated in the volume *V* by laser beam.

2.1.3. TIME INTEGRATION METHOD

In transient heat conduction analysis, Eq. (13) must be integrated over the time. Different time integration methods based on one or more-time steps are available. In this work, the method adopted is a one-time step method, often named the generalized trapezoidal method. This time integration method can be deduced from the Taylor's expansion series, by neglecting the second and higher-orders terms and introducing a time weighting factor α varying between 0 and 1. Thus, the temperature field at instant t+Δt is obtained (Eq. (18)) the following equation:

$$\mathbf{T}_{t+\Delta \mathrm{f}} = \mathbf{T}_{\mathrm{t}} + [\alpha \dot{\mathbf{T}}_{\mathrm{t}+\Delta \mathrm{t}} + (1 - \alpha)\dot{\mathbf{T}}_{\mathbf{t}}]\Delta t. \quad \textbf{(18)}$$

Applying the definition of the trapezoidal method into Eq. (13), the following expression (Eq. (19)) is obtained:

$$\begin{aligned} \left[\frac{1}{\Delta t}\mathbf{C} + \alpha\left(\mathbf{K}_{\mathrm{cond}} + \mathbf{K}_{\frac{\mathrm{conv}}{\mathrm{rad}}}\right)\right]\mathbf{T}_{t+\Delta t} & \\ - \left[\frac{1}{\Delta t}\mathbf{C} - (\mathbf{1} - \alpha)\left(\mathbf{K}_{\mathrm{cond}} + \mathbf{K}_{\frac{\mathrm{conv}}{\mathrm{rad}}}\right)\right]\mathbf{T}_t & \\ = (1-\alpha)\mathbf{Q}_t + \alpha\mathbf{Q}_{t+\Delta t} + (1-\alpha)\mathbf{f}_t + \alpha\mathbf{f}_{t+\Delta t}. & \end{aligned} \quad \textbf{(19)}$$

Depending on the value selected for α, the generalized trapezoidal method takes the form of well-known time integration methods such as, Euler forward method (α=0), Crank Nickolson method (α=$\frac{1}{2}$), Galerkin method ($\alpha = \frac{2}{3}$) and Euler backward method (α=1).

Only the Euler backward is known to be unconditionally stable for non-linear thermal problems, i.e. starting from a thermal equilibrium state at time *t,* it

reaches a thermal equilibrium state at time $t+\Delta t$. Therefore, assuming (α=1), Eq. (19) takes the following form:

$$\left[\frac{1}{\Delta t}\mathbf{C}+\left(\mathbf{K}_{\text{conv}}+\mathbf{K}_{\overline{\text{rad}}}^{\text{conv}}\right)\right]\mathbf{T}_{t+\Delta t}-\left(\frac{1}{\Delta t}\mathbf{C}\right)\mathbf{T}_{t} = \mathbf{Q}_{t+\Delta t}+\mathbf{f}_{t+\Delta t}, \tag{20}$$

which is typically solved with the Newton-Raphson iterative method, guaranteeing the equilibrium in all increments. The non-linear system presented in Eq. (21) can be rewritten in a simplified way, as follows:

$$\mathbf{K}_{\text{G}}\mathbf{T}_{t+\Delta t}-\mathbf{P}_{t+\Delta t}=\mathbf{R}_{t+\Delta t}, \tag{21}$$

where $\mathbf{K}_{\text{G}}$ and $\mathbf{P}_{t+\Delta t}$ (Eqs. (22) and (23)) assume the following form:

$$\mathbf{K}_{\text{G}}=\frac{1}{\Delta t}\mathbf{C}+\left(\mathbf{K}_{\text{cond}}+\mathbf{K}_{\overline{\text{rad}}}^{\text{conv}}\right), \tag{22}$$

$$\mathbf{P}_{t+\Delta t}=\left(\frac{1}{\Delta t}\mathbf{C}\right)\mathbf{T}_{t}+\mathbf{Q}_{t+\Delta t}+\mathbf{f}_{t+\Delta t}, \tag{23}$$

and $\mathbf{R}_{t+\Delta t}$ is the residue originated by the updating of $\mathbf{K}_{\text{G}}$ and $\mathbf{P}_{t+\Delta t}$ with the temperature distribution for the instant $t+\Delta t$.

The application of Newton-Raphson iterative scheme involves the evaluation of the linearized system of Eq. (22), which is expressed by:

$$\begin{aligned}\left(\frac{1}{\Delta t}\mathbf{C}_{t+\Delta t}^{i}+\mathbf{K}_{t+\Delta t}^{i}\right)\Delta\mathbf{T}_{t+\Delta t}^{i+1} &= \left(\frac{1}{\Delta t}\mathbf{C}_{t+\Delta t}^{i}\right)\mathbf{T}_{t}+\mathbf{Q}_{t+\Delta t}^{i}+\mathbf{f}_{t+\Delta t}^{i} \\ &-\left(\frac{1}{\Delta t}\mathbf{C}_{t+\Delta t}^{i}+\mathbf{K}_{t+\Delta t}^{i}\right)\mathbf{T}_{t+\Delta t}^{i},\end{aligned} \tag{24}$$

Where the superscript *i* and the subscript *t*, which follow the vectors and matrices, represent the iteration number and the configuration where the vectors and matrices are calculated, respectively. The matrix **K** is given by [20].

$$\mathbf{K} = \mathbf{K}_{\mathrm{cond}} + \mathbf{K}_{\mathrm{conv/rad}}. \quad \textbf{(25)}$$

The adoption of a fully implicit method (Newton-Raphson) presents the drawback of excessive computational cost, contrasting with explicit and semi-implicit methods such as Euler's method, Crank Nickolson's method and Galerkin's method. However, implicit algorithms guarantee the equilibrium in all increments, leading to stable results.

2.2. ELEASTOPLASTIC MATERIAL BEHAVIOR

In order to obtain the mechanical response of the workpiece during the manufacturing process, the *quasi*-static mechanical analysis is carried out using the current temperature field (obtained from the thermal analysis). The balance of linear momentum in any point of the boy (Eq. (26)) (part to be manufactured) is given by:

$$\mathrm{div}(\boldsymbol{\sigma}) + \mathbf{b} = \mathbf{0} \quad \textbf{(26)}$$

where **σ** is the stress tensor and **b** are the body forces, which are neglected in the present model. Regarding the boundary conditions, prescribed displacements are imposed on the Dirichlet boundary [21]. As is well known, thermophysical properties are temperature dependent, thus, they have to be specified according to the temperature [14].

The total strain increment (Eq. (27)) is the superposition of the following terms:

$$\Delta\varepsilon^{\mathrm{total}} = \Delta\varepsilon^{\mathrm{e}} + \Delta\varepsilon^{\mathrm{p}} + \Delta\varepsilon^{\mathrm{th}} \quad \textbf{(27)}$$

where $\Delta\varepsilon^{e}$ is the elastic strain increment, $\Delta\varepsilon^{p}$ is the plastic strain increment and $\Delta\varepsilon^{th}$ is the thermal strain increment. The effects of strains induced by solid-state phase transformation and creep are neglected in the present model.

The linear elastic constitutive law defines a linear relationship between the stress tensor and the strain tensor. Thus, the resulting stress from the elastic strain is expressed as:

$$\boldsymbol{\sigma}^{\mathbf{e}} = \mathbf{C} : \boldsymbol{\varepsilon}^{\mathbf{e}} \tag{28}$$

where **C** is the fourth-order material stiffness tensor (Elastic moduli). Assuming an isotropic linear elastic material, the stiffness matrix **C** can be calculated from the Young's modulus (*E*) and the Poisson's ratio (*v*).

Considering an associated flow rule in the plasticity model, the plastic strain increment is given by:

$$\Delta\varepsilon^{\mathrm{p}} = \lambda \frac{\partial f}{\partial \sigma} \tag{29}$$

where λ is the plastic multiplier, which is calculated through the consistency condition. The plastic behaviour is also assumed as isotropic, described by von Mises yield criteria. Hence the yield function *f* is obtained by:

$$f = \sigma_{\mathrm{vM}} - \sigma_{\mathrm{y}} \leq 0 \tag{30}$$

where σ_{vM} represents the von Mises equivalent stress and σ_y is the yield stress.

In this study, the phenomenological Swift law is adopted to describe the hardening of the material. The parameters of the Swift law are considered temperature dependents in order to take into account the strong impact of the temperature on the mechanical behaviour of the material.The isotropic work hardening function is given by:

$$\sigma_{\mathrm{y}} = K(\varepsilon_0 + \varepsilon^{\mathrm{p}})^n \tag{31}$$

where *K*, ε_0 and *n* are the material parameters, while ε^{p} denotes the equivalent plastic strain. The initial yield stress is defined by $\sigma_0 = K(\varepsilon_0 + \bar{\varepsilon}^{\mathrm{p}})^n$.

The total thermal strain is calculated as:

$$\varepsilon^{\mathrm{th}} = \left(\alpha_{\mathrm{T}}(T - T_{\mathrm{ref}}) - \alpha_{\mathrm{ini}}(T_{\mathrm{ini}} - T_{\mathrm{ref}})\right)\mathbf{I} \quad (32)$$

where α_T and α_{ini} are the volumetric thermal expansion coefficients evaluated at the current temperature T and at the initial temperature T_{ini}, respectively. T_{ref} is the reference temperature used to define the thermal expansion coefficients and I denotes the second-order identity tensor [21].

2.3. STAGGERED THERMO-MECHANICAL COUPLING

This section contains the staggered algorithm used in this study for coupling the thermal and mechanical solutions. This coupling algorithm was proposed in [22], to reach a better equilibrium between computational time and accuracy of results. The main difference to the classical staggered algorithms is the way that the information between the problem fields is interchanged.

The adopted algorithm is divided into two phases, a prediction phase and a correction phase, as is shown in Figure 4. The prediction phase aims to give a trial solution for the problem, which is not accurate, but assures an improvement of the convergence rate during the iterative procedure in the single field problems, performed using an implicit approach.

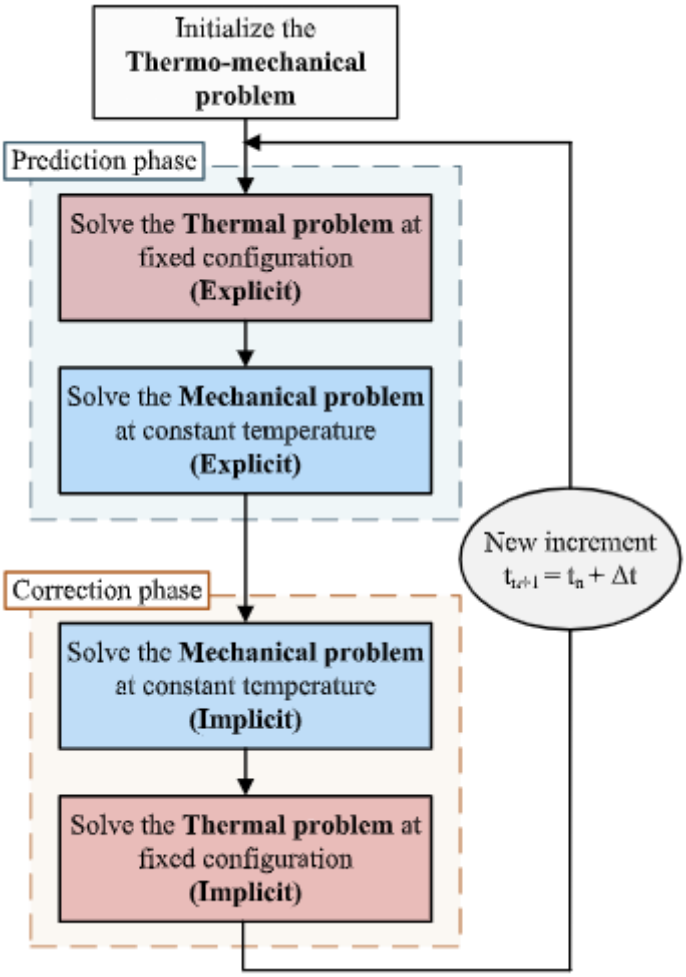

Figure 4: *Algorithm adopted for the thermo-mechanical coupling.*

2.4. NON-CONFORMING FINITE ELEMENT MESHES

Automatic generation of meshes is very demanding for creating complex real-world computational models. In general, the accuracy of a FEM solution using hexahedron mesh is satisfactory, provided the quality of the mesh is high. At present, the commonly used methods for generating unstructured hexahedral meshes include mapping method, plastering method, octree-based method, sweeping method and whisker weaving. In many hexahedral mesh generation techniques, the octree-based methods are still the most effective from an engineering practice point of view. Although a lot of efforts have been made, it remains a great challenge to generate quality pure-hexahedral meshes for complicated geometries. Due to inherited difficulties in topology [23].

Dramatic computational savings can be obtained when finite element meshes are graded in the neighbourhood of localized phenomena such as point loads, point supports, re-entrant corners, crack tips and heat sources [24].

Isoparametric quadrilaterals and hexahedrons for two-dimensional (2D) and three-dimensional (3D) mesh-grading algorithms are presented. They are computationally efficient, easily implemented in existing finite element programs and need not to be distorted in the grading process. The hexahedrons are the first 3D elements which can be graded efficiently and without distortion [24].

Octrees enable producing hexahedral meshes with different element sizing. However, the resulting meshes contain hanging nodes, which present challenges to some numerical solvers. The presence of hanging nodes also complicates the process of sharp feature extraction and subsequent mesh optimization steps [25].

2.4.1. MESH REFINEMENT WITH HANGING NODES

General mesh refinements may either maintain the conformity of the mesh or lead to irregular, non-conforming meshes. Irregular meshes involve ‘hanging nodes’ that are also referred to as ‘irregular vertices’. The differences between these two approaches are mainly found in the complexity of the refinement algorithm and the need for changes in the simulation codes that process the refined meshes.

For irregular meshes, one may specify the irregularity index *k* which denotes the maximum difference of refinement levels between adjacent elements in the mesh. The meshes used in this work are (symmetric) 1-irregular. That is, for bilinear elements, only one hanging node is accepted at the centre of an element edge. This is also called the 2-to-1 condition/property. A graphical representation of these irregular meshes is given in Figure 5 [26] .

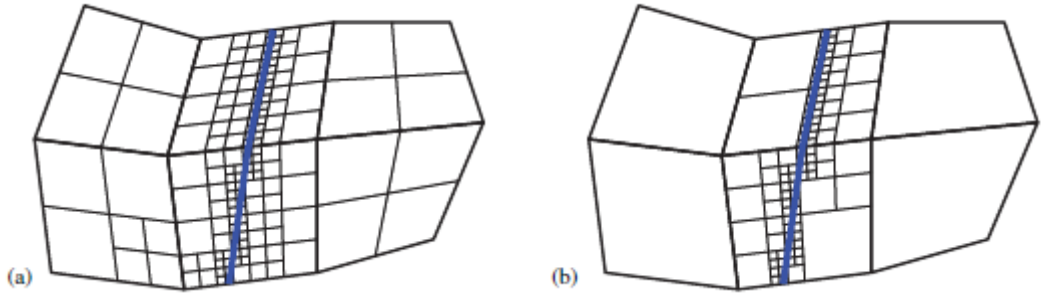

Figure 5: *Examples for irregular meshes that are refined at the interface: (a) 1-irregular mesh and (b) k-irregular mesh with k> 1. Only 1-irregular meshes as shown in (a) are used in this work.*

2.4.2. OCTREE MESH GENERATION

Octrees are widely used in computational sciences, due to its conceptual simplicity and ability to scale across large number of processors [27]. The generation of a hexahedral mesh based on the octree algorithm roughly consists in three steps. First of all, a uniform background grid is generated to cover the model. The octree background greed may be refined in some specified regions. Some of the typical refinement criterion may apply:

1. Boundary of the model.
2. Sharp ridges and corners of the model.
3. The surface area with a high curvature.
4. The region with stress concentration.

Balance conditions ned to be met during the mesh generation process to ensure desired accuracy. The octree grid is balanced so that the maximum size ratio between adjacent octree cells is 2. This operation will simplify the cases to several patterns and provide a smooth mesh-size transition. There is at most one hanging node on each edge of the mesh, and the dimensions between adjacent elements are generally capped at 2. This prevents too heavy distortion caused by different sizes over the entire mesh. A typical case of comparison between unbalanced and balanced octree grid is shown in Figure 6 [23].

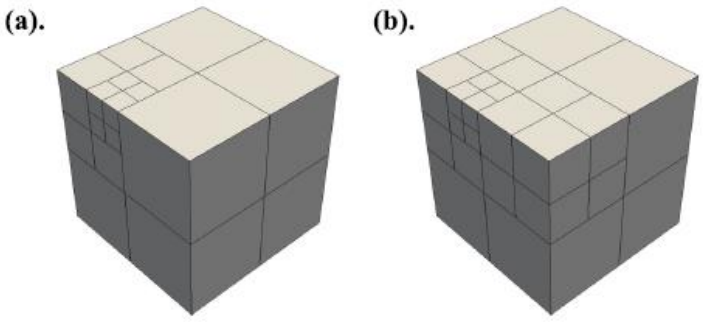

Figure 6: *Octree grid balancing: (a) unbalanced octree and (b) balanced octree.*

Upon octree generation we enforce the 2:1 balanced constraint which ensures that neighbouring octants differ by at most one level. Such a 2:1 balanced constraint simplifies mesh generation, and eliminates ill-conditioning introduced due to extreme scaling of neighbour elements.

3. NUMERICAL MODEL

Some problems appear in the manufacturing of the SLM process and in this section will be develop the numerical model of the Selective Laser Melting process. A better understanding of SLM is required to minimize these defects and allow for its full adoption by industry.

3.1. IN HOUSE FINITE ELEMENT CODE DD3IMP

The numerical simulations were carried out with the in-house finite element code *DD3IMP*, originally developed to simulate sheet metal forming processes [21]. The main featuress of the finite element code are the next ones:

- Large elastoplastic strains and rotations.
- Updated Lagrangian scheme.
- Transient thermal analysis volumetric heat source
- Heat losses by convection and radiation
- Fully implicit algorithm with Newton-Raphson method.
- Thermo-mechanical coupling using a staggered algorithm.
- Temperature dependent material properties.
- Library of solid finite elements
- Non-conforming meshes.
- OpenMP directives.

All the results obtained in the simulations have been obtained on a desktop computer provided with *Intel® Core™ i7-2600K 3.40GHz 8GB RAM* except the simulation of the conforming fine mesh that was obtained with *Intel® Core™ i7-4770K 3.50GHz 16GB RAM.* For the pre-processing and the postprocessing it has been used *GID* program.

3.2. SINGLE-LAYER AND SINGLE-TRACK EXAMPLE

This section presents the single-layer and single-track example adopted to analyse the SLM process. In order to reduce the computational cost associated with the numerical simulation, the domain considered for the SLM process was

significantly decreased. A single powder layer was studied considering a single-track deposition. This single layer was scanned over substrate to enable thermomechanical conditions like the ones obtained in the SLM. In this study, the substrate bottom is fixed during SLM processing, including after cooling down.

Three models have been used for this study (Figure 8), two with a conforming mesh and the other one with a non-conforming mesh. Figure 7 presents, the geometry and dimensions used for the simulations, including the axis definition. The part in grey is the baseplate and the blue one is the powder layer. The process parameters that are used in this simulation appear in the Table 3. The distance that the laser travels, is less than the length of the baseplate, there is 0.2 mm on each side. These properties and process definition were extracted from [28], for a single laser track using SLM process.

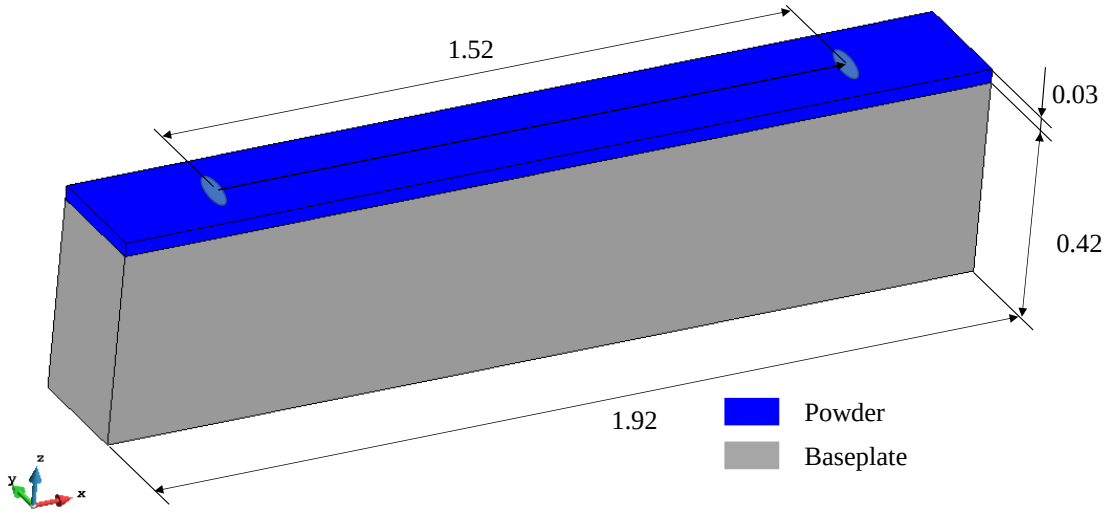

Figure 7: *Single laser track domain (dimensions in mm).*

Table 3: *SLM process parameters.*

Parameters	value
Laser power P [W]	200
Laser speed [mm/s]	800
Laser spot radius [μm]	50
Laser depth [µm]	150
Powder layer thickness [µm]	30
Emissivity ε	0.6
Room temperature [K]	308

Since the SLM process initially comprises the material phase transformation from powder to liquid, which the cools down to solidification, three material phases were considered in the simulation: powder, liquid and solid. The powder material switches to liquid when the temperature rises to the melting point (1923K) and the liquid material solidifies when the temperature cools down to the melting point (bidirectional transformation). Moreover, each material phase requires a set of temperature dependent material properties, particularly those with a more pronounced variation in this temperature range. However, the allotropic transformation occurring in the Ti-6Al-4V at elevated temperatures is neglected in the model, which simplifies the thermo-mechanical analysis of the solid phase material [21].

The temperature dependant material properties of the solid Ti-6Al-4V are listed in Table 4, namely the specific heat capacity, thermal conductivity, thermal constant coefficient, Young modulus and the Poisson's ratio. Both the Poisson's ratio and the mass density are assumed constant in the numerical simulation[19]. The thermal expansion is the root cause of residual stresses and part distortion,

but its effect on the thermal field is almost negligible Except thermal conductivity, all thermal and physical properties of the liquid phase are assumed constant in the numerical simulation (see

Table 5)

Table 4: *Temperature-dependent material properties of solid Ti-6Al-4V.*

Temperature [K]	Density ρ [g/cm³]	Specific heat capacity c_p [J/kg K]	Thermal conductivity *k* [W/m K]	CoTE α [1/K]	Young modulus [MPa]	Poisson's ratio *v*
293	4.30	543	7.07	8.80 E-06	125000	0.34
500	4.30	566	9.3	1.20 E-05	100000	0.34
950	4.30	646	15.3	1.20 E-05	55000	0.34
1061	4.30	665	17	1.20 E-05	20000	0.34
1172	4.30	685	18.5	1.20 E-05	10000	0.34
1394	4.30	760	24	1.20 E-05	3000	0.34
1950	4.30	820	27	1.20 E-05	50	0.34
2000	4.30	820	27	0	50	0.34

Table 5: *Temperature-dependent material properties of liquid Ti-6Al-4V.*

Temperature [K]	Density ρ [g/cm^3]	Specific heat capacity c_p [J/kg K]	Thermal conductivity *k* [W/m K]	CoTE α [1/K]	Young modulus [MPa]	Poisson's ratio *v*
1950	4.3	820	27	0	50	0.34
3300	4.3	820	55	0	50	0.34

The mass density of the powder, liquid and solid are assume constant. Nevertheless, the mass density of the powder is 60% of the solid Ti-6Al-4V, due to the assumption of 0.6 for the packing factor of the powder bed [21] (see

Table 5Table 6). Powder has a lower conductivity with respect to the solid phase, depending on porosity, pore geometry, and filling gas [19]. Thus, the thermal conductivity for the powder is assumed roughly 10 times smaller than that of the same bulk material due to the porosity of the powder bed.

Table 6: *Temperature-dependent material properties of powder Ti-6Al-4V.*

Temperature [K]	Density ρ [g/cm³]	Specific heat capacity c_p [J/kg K]	Thermal conductivity *k* [W/m K]	CoTE α [1/K]	Young modulus [MPa]	Poisson's ratio *v*
500	2.60	505	0.104	1.20 E-06	50	0.34
800	2.60	473	0.078	1.20 E-06	50	0.34
1100	2.60	507	0.279	1.20 E-06	50	0.34
1300	2.60	610	0.813	1.20 E-06	50	0.34
1600	2.60	951	1.27	1.20 E-06	50	0.34
1950	2.60	999	1.8	1.20 E-06	50	0.34

The increase of the temperature leads to a decrease of mechanical strength. Therefore, the hardening law is assumed temperature dependent, i.e. the parameters of the Swift law are assumed temperature dependent. The hardening coefficient of the Swift law (see eq. (31)) is assumed constant with the temperature, and it is identical for all material phases (see Table 7). The K in the Table 7 for the Swift law, is roughly 2 times the Yield stress.

Table 7*: Temperature-dependant mechanical properties for the Ti-6Al-4V material.*

Temperature [K]	Yield Stress [MPa]	K [MPa]	n
293	1000	2000	0.35
500	630	1500	0.35
950	300	770	0.35
1172	55	120	0.35
1394	17	60	0.35
1950	1.5	10	0.35

3.3. FINITE ELEMENT MODEL

This section, contains the definition of the boundary conditions, discretization, number of increments and the numerical parameters. The model used for the simulation is cut from the middle in the XZ plane, with the aim of have less computational time by take advantage of the symmetry conditions. A boundary condition has been added in this plane, in order to simulate the symmetry condition. This boundary condition restrains the movement of this face t in the *y* direction.

In order to assess the effect of the finite element mesh on the accuracy of the numerical solution, three different discretization are adopted in the present study. The conforming fine mesh (Figure 8 a)) presents the same element size in all volume. The total number of finite elements and nodes is present in Table 8 for each mesh adopted. The conforming mesh with gradient in the mesh size

(Figure 8 b)) have smaller elements in the top part in order to have accurate results in the area that the laser hits. The larger gradients in the stress and temperature arise around the top surface due to the position of the heat source. The non-conforming mesh have 4 different sizes of elements. The area corresponding to the smaller mesh size is bigger than in the conforming mesh, but this mesh has less elements and nodes (see Table 8). The non-conforming mesh have the smallest elements only in the area that the laser hits, improving the definition of gradients caused by the heat source.

Table 8: *Number of nodes and elements of each mesh.*

	Conforming fine mesh	Conforming mesh with gradient	Non-conforming mesh
nº nodes	22371	15971	11648
nº elements	131072	49152	31008

The simulations contain 2 different phases: laser track and cooling. It has been defined a number of increments for each phase. The laser track has 200 increments and the cooling 333 increments. During the cooling phase the laser power is turned off in order to decrease the temperature and consequently generate the strong residual stresses.

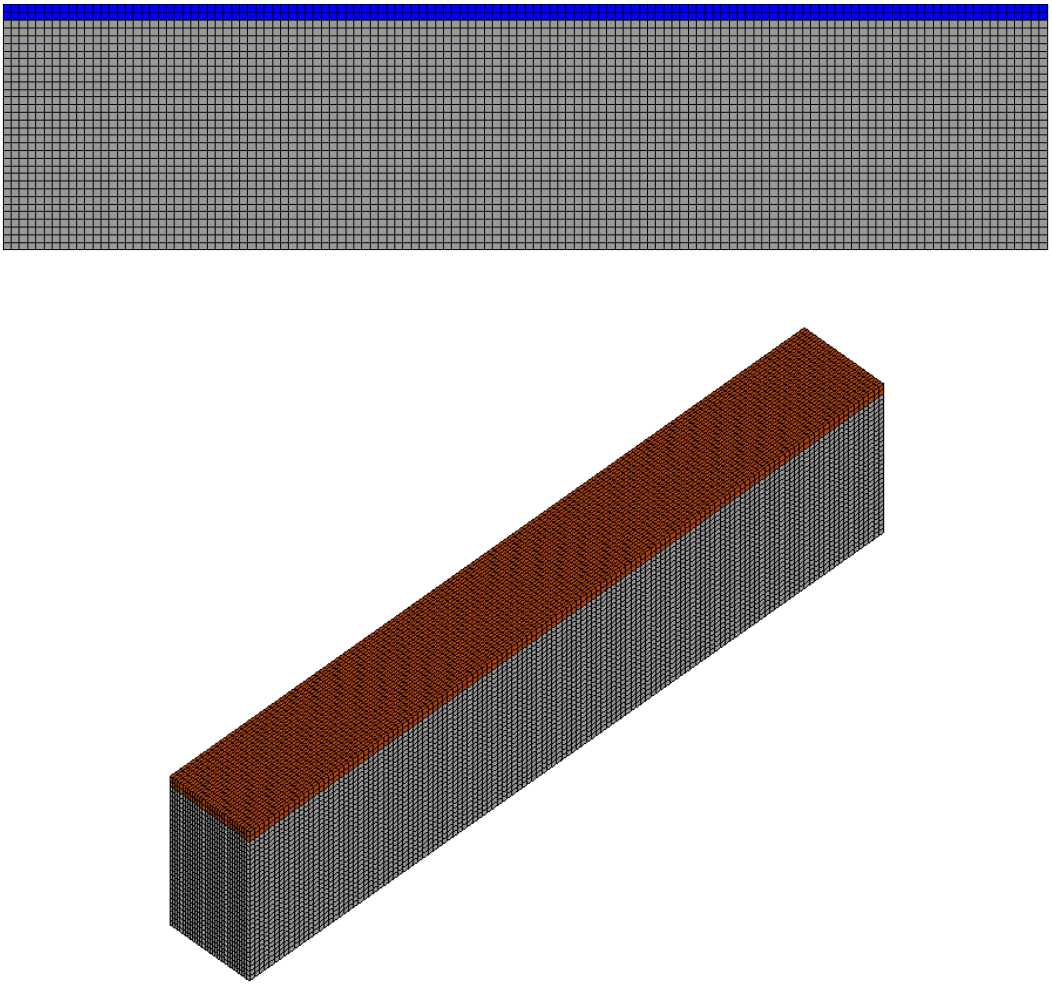

a) Conforming fine mesh

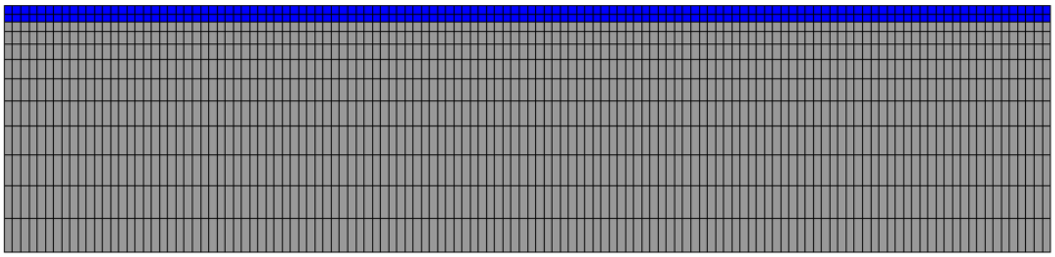

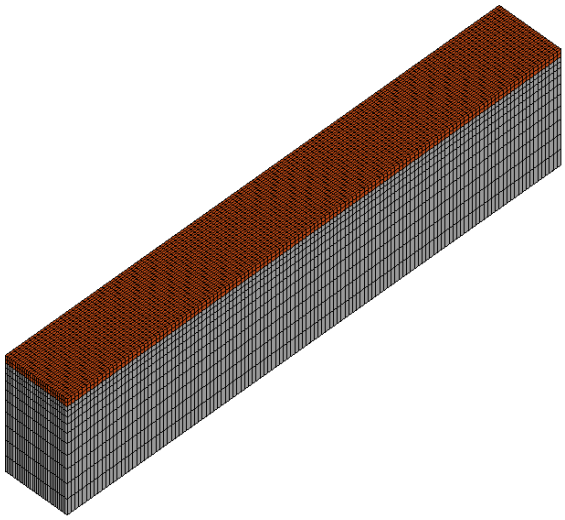

b) Conforming mesh with gradient

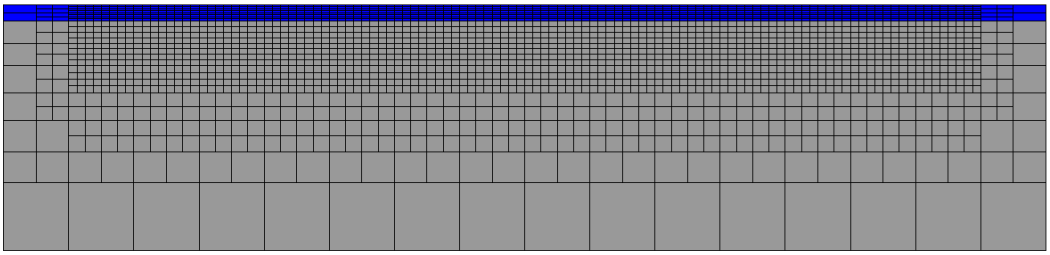

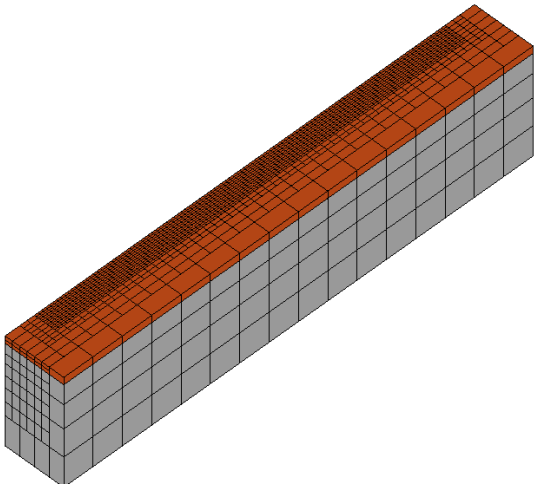

c) Non-conforming mesh

Figure 8:*Lateral view of the finite element meshes used in the thermo-mechanical simulation.*

4. RESULTS AND DISCUSSION

This section contains the main result obtained with the finite element model previously presented (Figure 7). The results are mainly analysed at the middle of the laser track in the upper part, see Figure 9 (the red point is where the results of the graphs have been obtained). First of all, the thermal model has been analysed in order to validate that the simulation results and then the mechanical simulation has been performed as its mentioned before.

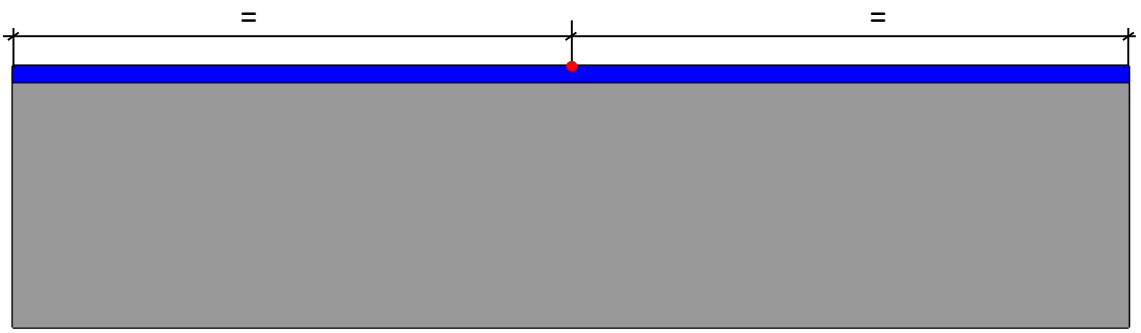

Figure 9: *Definition of the point where the temperature, stress and strain have been obtained.*

The results obtained in this study will be compared with the experimental and numerical measurements of the Table 9. These measurements refer to the dimensions of the melt-pool. In the present study, the melt pool is defined by the region with temperature, over 1923 K, which, is the melt temperature for the *Ti-6Al-4v* material.

Table 9: *Melt-pool width and depth values: comparison between the experimental measurements reported in* [28] *and the numerical model validated in* [28].

	Measurement [28]	Autodesk®Netfabb™ [28]
Width [µm]	180	195
Depth [µm]	140	110

4.1. THERMAL MODEL VALIDATION

The depth, width and length of the melt-pool is defined by temperature distribution provided by the thermal simulation. On the other hand, the accuracy of the numerical solution is influenced by the mesh quality. Thus, the computational time of the thermal analysis is assessed before starting the analysis of residual stresses through the thermomechanical model. Figure 10, shows the geometry and the dimensions of the melt pool when the laser is located in the centre point of the single laser track. The white area depicts the melt pool, i.e. this region presents temperatures over 1923K.

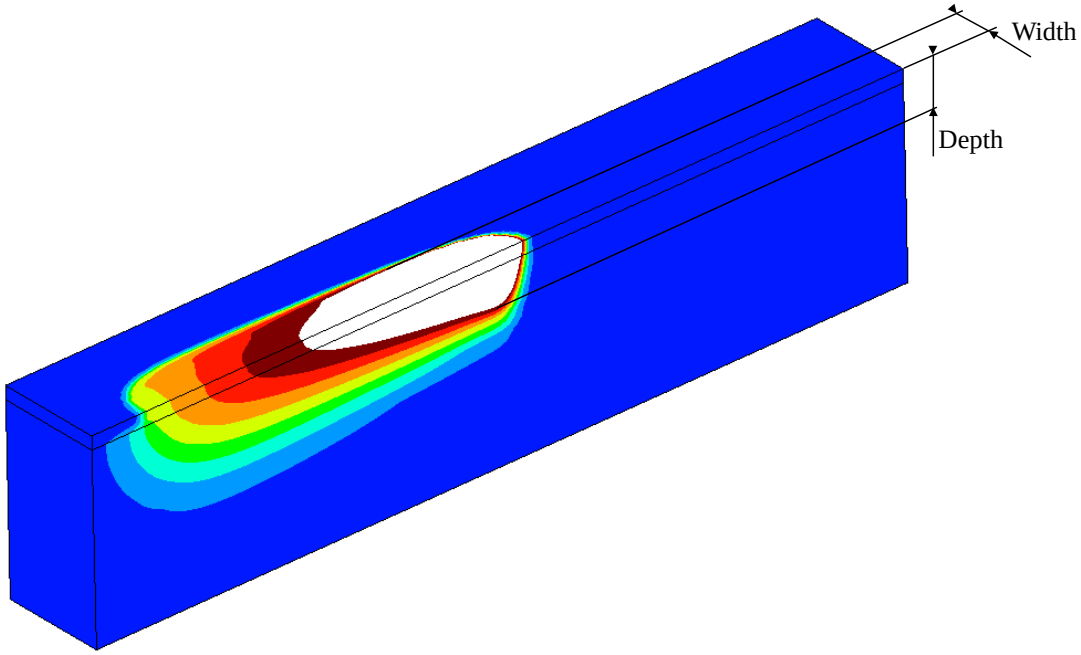

Figure 10: *Melt pool dimensions*

Table 10 presents the comparison of the obtained results using different meshes. The results are very similar in temperature, as well as in the dimensions of the melt pool (depth and width). The biggest difference appears in the computational time, i.e. the conforming mesh needs about 18% more of time that the non-conforming mesh. The conforming mesh have much more nodes and elements (see Table 8), requiring more computational time. The aim of the non-conforming mesh is that most of the nodes and elements are in the upper part of

the model, i.e. the location where the temperature has more impact and where we need more accuracy.

Table 10: *Computational performance and dimensions of the melt-pool obtained using two different meshes in the thermal simulation.*

	Time [h]	Percentage of the time	Temperature in the middle [K]	Depth [mm]	Width [mm]
Non-conforming mesh	0:16:15	100%	5016	0.1115	0.165
Conforming mesh	0:19:16	118%	5031	0.1159	0.165

4.2. THERMO-MECHANICAL MODEL SIMULATION

After analysing the thermal model (temperature distribution), the residual stresses have been analysed using the thermomechanical model. For visualization purposes, the meshes have been deleted in the presentation of the results. Moreover, the 9-color scale has been chosen in order to achieve more accurate and visual results. In this way, critical areas can be located and identified in a more visual way.

Although the adopted meshes are identical to the ones previously used in the thermal analysis, the computational time needed for the mechanical simulation in higher than in the thermal simulation. The number of nodes and elements for this simulation is the same but the number of degrees of freedom is larger (see Table 11**¡Error! No se encuentra el origen de la referencia.**). The thermomechanical analysis comprises nodal temperatures and nodal displacements, while the thermal analysis only involves the temperature.

For this thermo-mechanical simulation, another mesh has been created and analysed. This new mesh is also a conforming mesh, the difference between both conforming meshes is that this one is finer than the older. Using this new

mesh, more accurate result is going to be obtained, on the other hand, requires a bigger computational time, as is shown in Table 11.

The aim of this new mesh is to see how much more time is needed with a conforming mesh to obtain the same results that with the non-conforming mesh.

Table 11: *Computational performance and dimensions of the melt pool obtained using different meshes in the thermo-mechanical simulation.*

	Time [h]	Percentage of the time	Depth [mm]	Width [mm
Non-conforming mesh	8:05:20	100%	0.1115	0.18
Conforming mesh	31:09:11	385%	0.1159	0.172
Conforming fine mesh	154:07:04	1905%	0.114	0.173

First, it is analysed the temperature distribution when the laser is located in the middle of the scan track (see Figure 9). As in the thermal problem, the difference in terms of predicted temperature is negligible (see Figure 11). However, in the difference in the computational time is significative, as mentioned before (see Table 11). The conforming mesh need around 3.85 times more time than the non-conforming mesh, while the conforming fine mesh requires around 19 times more time. Besides, it should also be borne in mind that the simulation of conforming fine mesh has been carried out in a different computer with better performance.

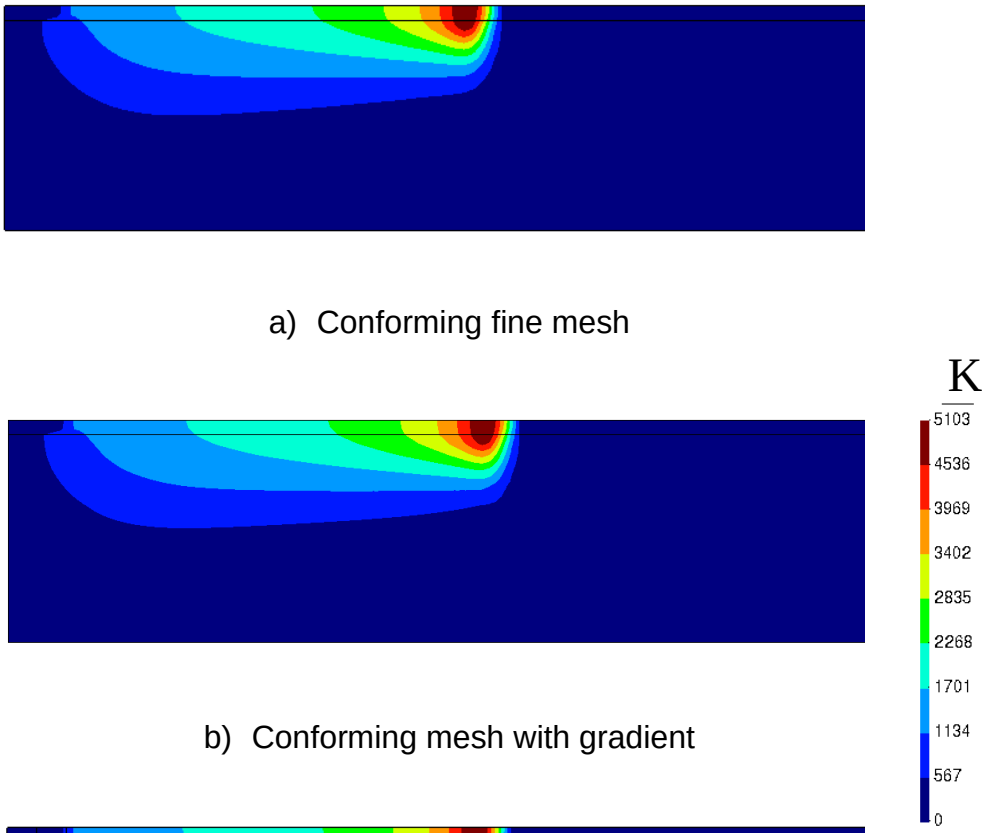

a) Conforming fine mesh

b) Conforming mesh with gradient

c) Non-conforming mesh

Figure 11:*Distribution of the predicted temperature when the lase in the middle of the track.*

The temperature distribution after cooling time is presented in Figure 12, comparing the solution obtained by each finite element mesh. This is not the real after cooling because the final temperature is higher than the room temperature. However, the temperature (Figure 13) presents an asymptote and it is assuming that the results are going to be very similar. On the other hand, the computational time required to get the room temperature will be high due to the number of time increments required. Therefore, the residual stresses are evaluated after 0.0075

seconds of cooling, which are assumed not change drastically by increasing the cooling time. The difference between meshes in the thermal problem is negligible, as highlighted in Figure 11 andFigure 12. The temperature of the deposited material layer is about 600K, which is significantly lower than the melting temperature.

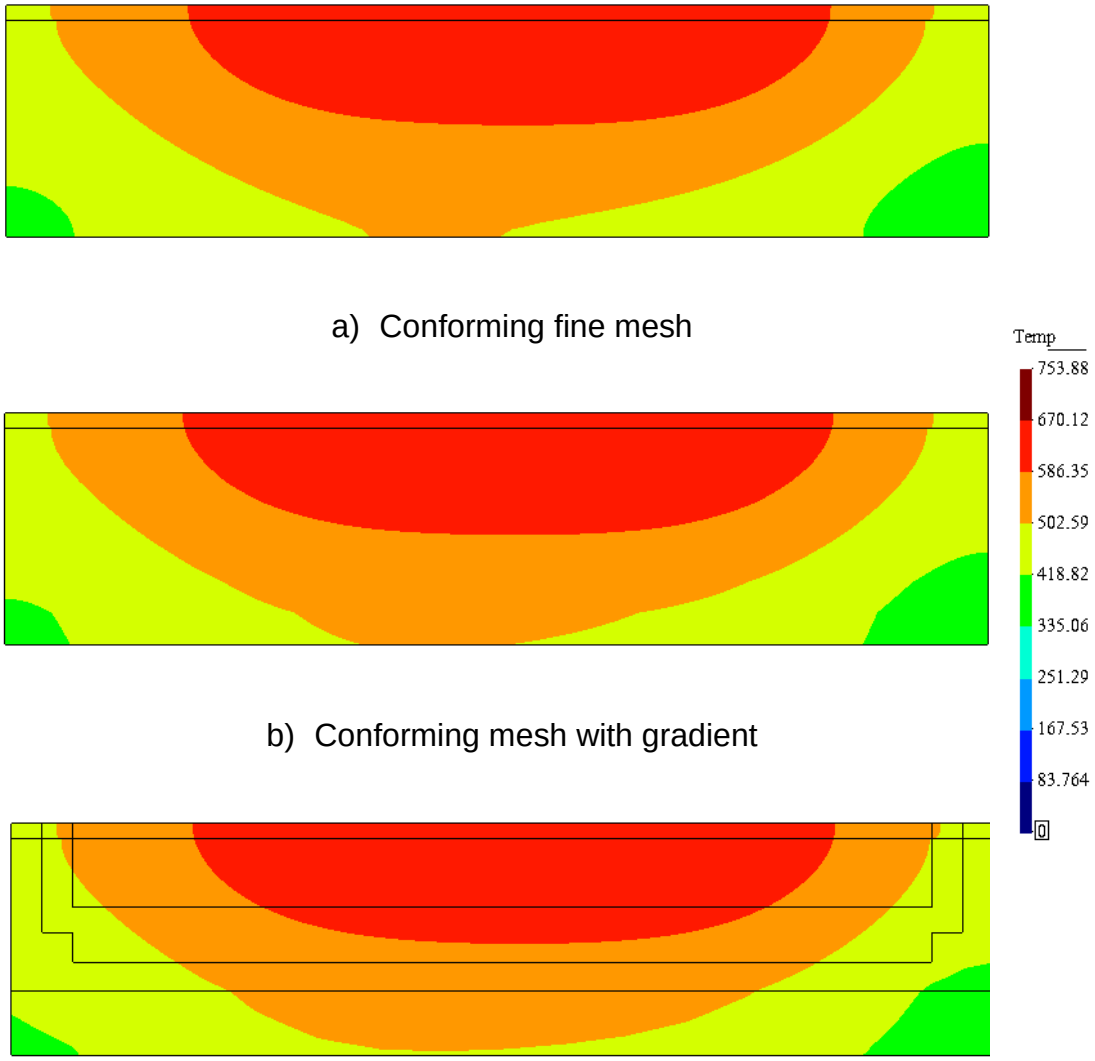

a) Conforming fine mesh

b) Conforming mesh with gradient

c) Non-conforming mesh

Figure 12: *Distribution of the predicted temperature after 0.0075 seconds of cooling.*

Figure 13 shows the temperature evolution along the time in the middle point (Figure 9), comparing the 3 meshes. The difference between the predicted

temperature is negligible between 3 meshes. This highlights that the mesh size used in all meshes is enough to capture accurately the thermal gradients around the heat source.

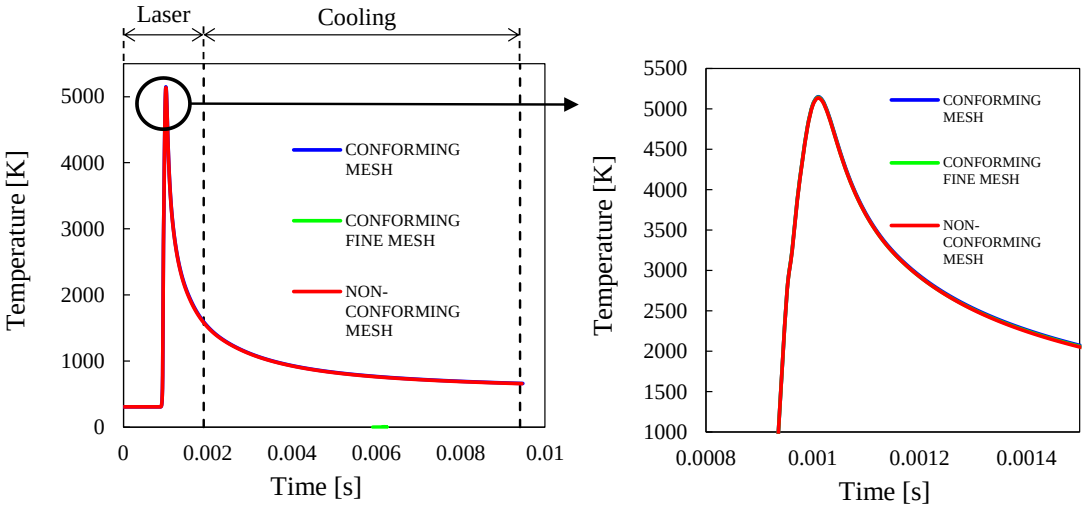

Figure 13: *Predicted temperature evolution in the middle point of the laser track, comparing both types of meshes.*

The plastic strain distribution after cooling is presented in Figure 14, comparing the results from different meshes. The region where arise the maximum values of plastic strain is not in the upper surface. Indeed, the plastic strain arises under the deposited layer, (inside of the piece), i.e. in the lower part of the melt pool. The non-conforming mesh is finer in that area, providing solutions. This is the reason because the non-conforming mesh show better distribution of the results. Considering the point shown in Figure 9, the difference between the plastic strain obtained with conforming and non-conforming mesh is21.5% (see Figure 15**¡Error! No se encuentra el origen de la referencia.**). On the other hand, the diference between the non-conforming mesh and the confrming fine mesh is negligible. Indeed, the distribution of the streeses in this both meshes is identical (as is shown inFigure 14 b).

The area where the laser hits firsts is the area that presents the high equivalent plastic strain. This large value of plastic strain is caused by the strong teemal gradients ocurring at the beginning since the initial temperature is lower. Then, the fast solidification of the liquid metal, creates internal stresses and consequently plastic strain in this region. Acording to the evolution of the plastic

strain in the middel point, a significant amount of plastic strain occurs during the cooling stage. The differences between the two conforming meshes appear mainly during the travel of the laser. Nevertheless, the final value is significantly different since the plastic strain is cumulative.

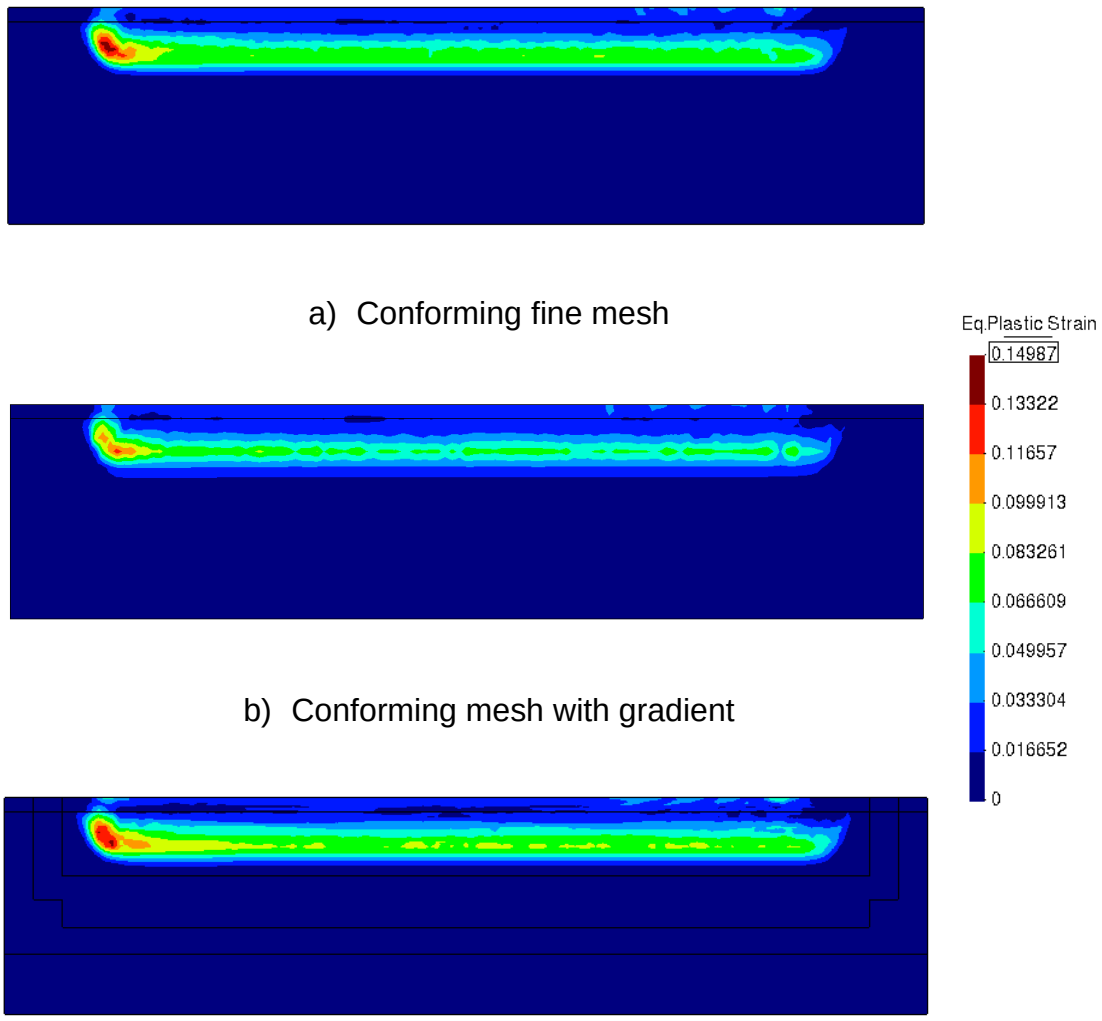

a) Conforming fine mesh

b) Conforming mesh with gradient

c) Non-conforming mesh

Figure 14: *Distribution of the predicted equivalent plastic strain after 0.0075 seconds cooling.*

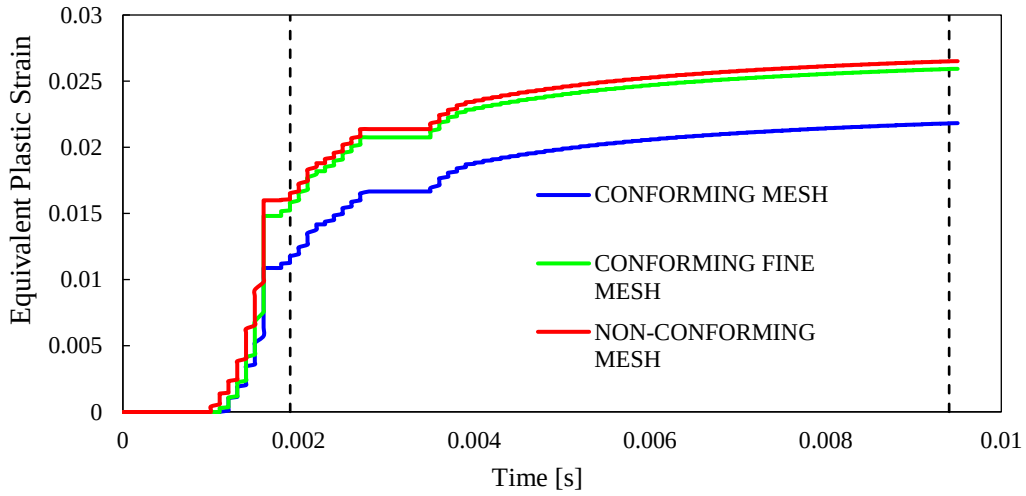

Figure 15: *Predicted equivalent plastic strain evolution in the middle point of the laser track, comparing both types if meshes.*

The distribution of the equivalent tensile stress is presented in Figure 16, comparing the different meshes adopted in the study. The Von Misses stress distribution seems smoother in the non-conforming mesh, which is similar to the conforming fine mesh. This is because where they appear the greatest stresses the non-conforming mesh is finer than the conforming one.

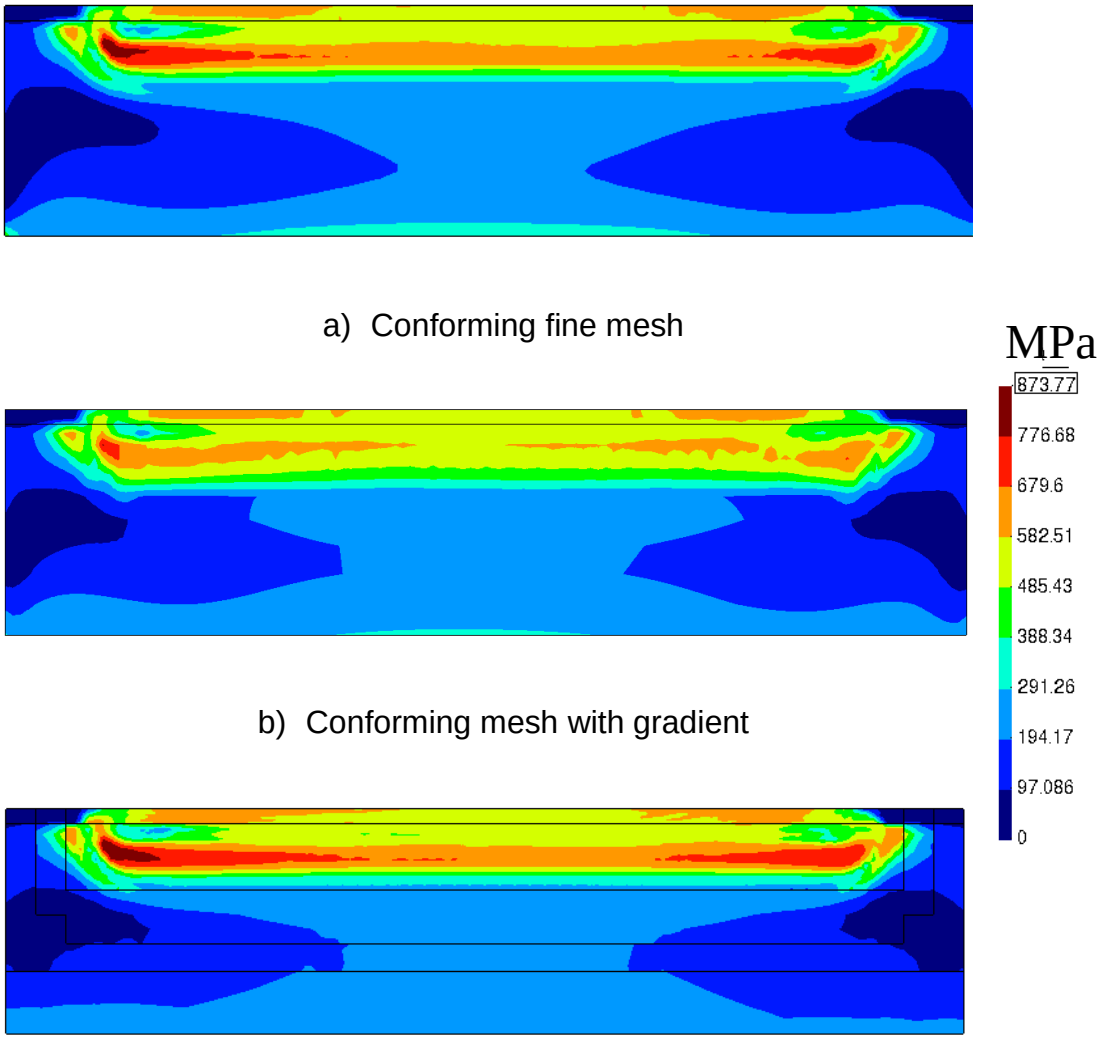

Figure 16: *Distribution of the predicted Von Mises stress after 0.0075 seconds cooling.*

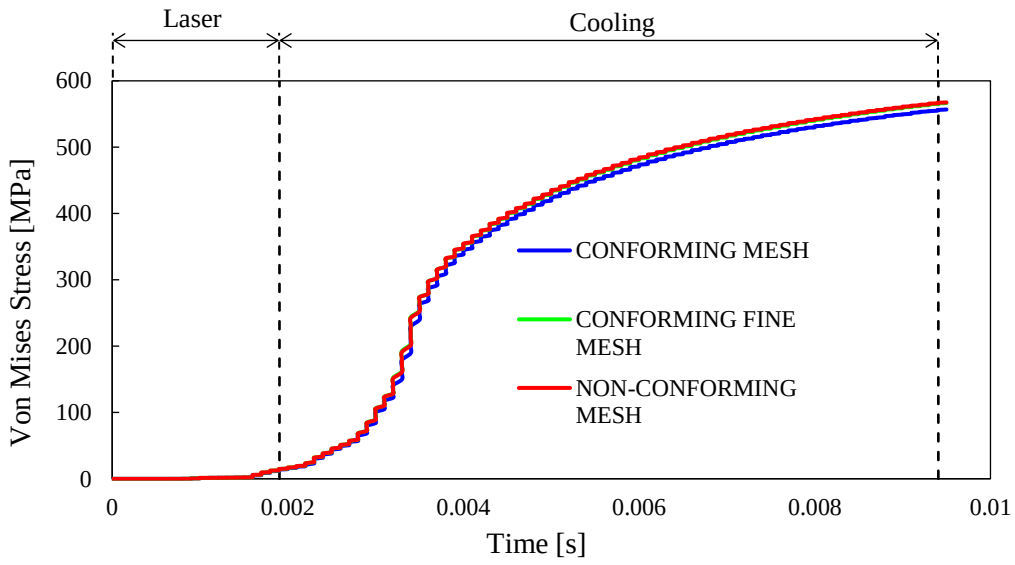

Figure 17: *Predicted Von Mises stress evolution in the middle point of the laser track, comparing both types of meshes.*

To have a better representation of the stresses along the piece, the results are represented also in three cuts in the YZ plane along the X direction. The first cut is C1 and is when the laser starts (x=0.2mm), the next one is in the middle (x=0.96mm) and the last one is when the laser finish (x=1.72mm). After cooling the largest stress is generated in the direction of the laser (X direction of the axes), see Figure 18. The stress change from compressive to tensile (in the deposited layer) rather than a steep gradient.

In the σ_{xx}, the maximum stress is 1518 MPa. As is mentioned before the laser impact deeper that in the powder layer. The non-conforming mesh have smaller elements also in the upper part of the baseplate and it is here where appear the highest stresses. The difference between the non-conforming mesh and the conforming one in the σ_{xx} after cooling, is around 8%.

The distribution of the σ_{xx} is more similar between the non-conforming mesh and conforming fine mesh (see Figure 18). This two meshes have smaller size of elements in the area of the laser impacts and the results and distribution are more accurate than in the conforming mesh. Regarding the computational time, the conforming fine mesh needs 19 times more of time than non-conforming mesh, as is shown in Table 8.

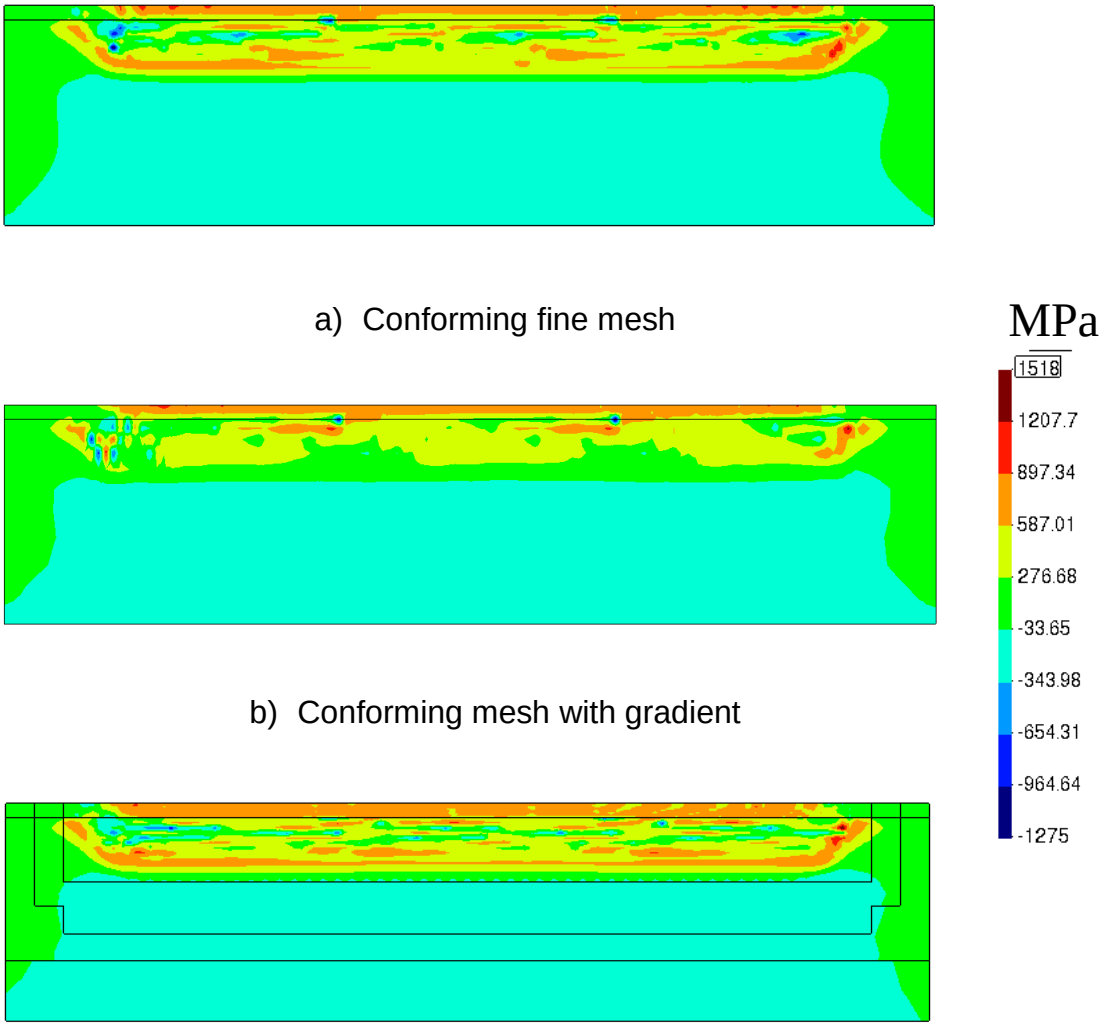

a) Conforming fine mesh

b) Conforming mesh with gradient

c) Non-conforming mesh

Figure 18: *Distribution of the predicted stress XX after 0.0075 seconds cooling.*

The difference between the 3 meshes is generated in the 0.0016 seconds and it is when the laser is in x = 1.45mm. The results are taking in x=0.96mm that is exactly in the middle of the piece. This difference is caused in the cooling phase, and it can be caused because as is shown in Table 7, between 950K and 1172K the yield stress difference is so high, more than in the other cases. At this time, the middle point is between these two temperatures mentioned before. The computers take the data as linear but is not linear so, two options are proposed in order to have better results. First one is to add more elements to the mesh. With this first option, the distance between nodes will be reduced and the iterations will be more accurate. The second option is to increment the number of

data, will be achieve better results because the difference in the Yield stress will be smaller. The most suitable will be to take both options into account at the same time, with this, the difference will be lower, and the results will be more accurate.

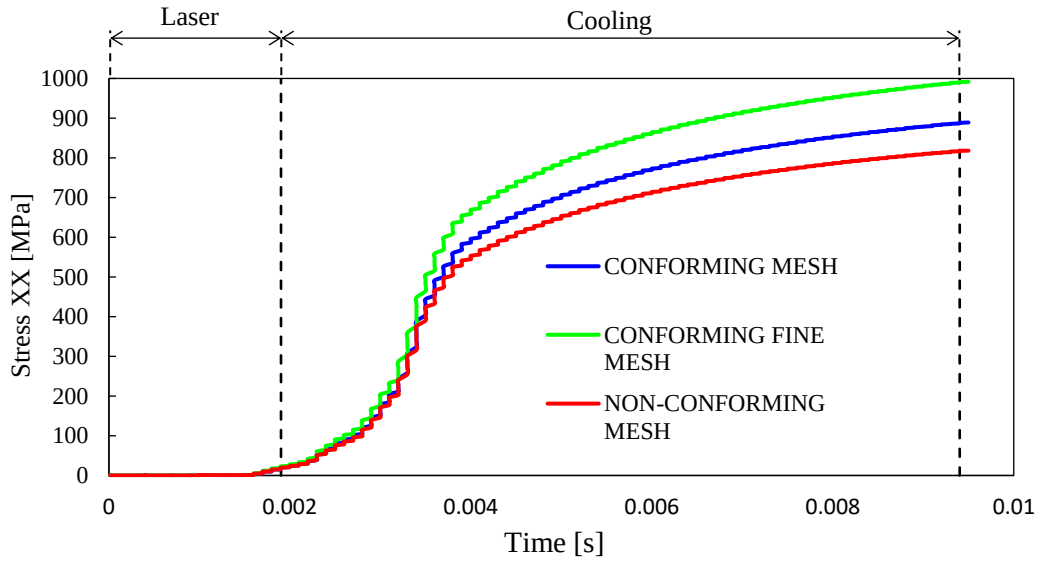

Figure 19: *Predicted stress XX evolution in the middle point of the laser track, comparing both types of meshes.*

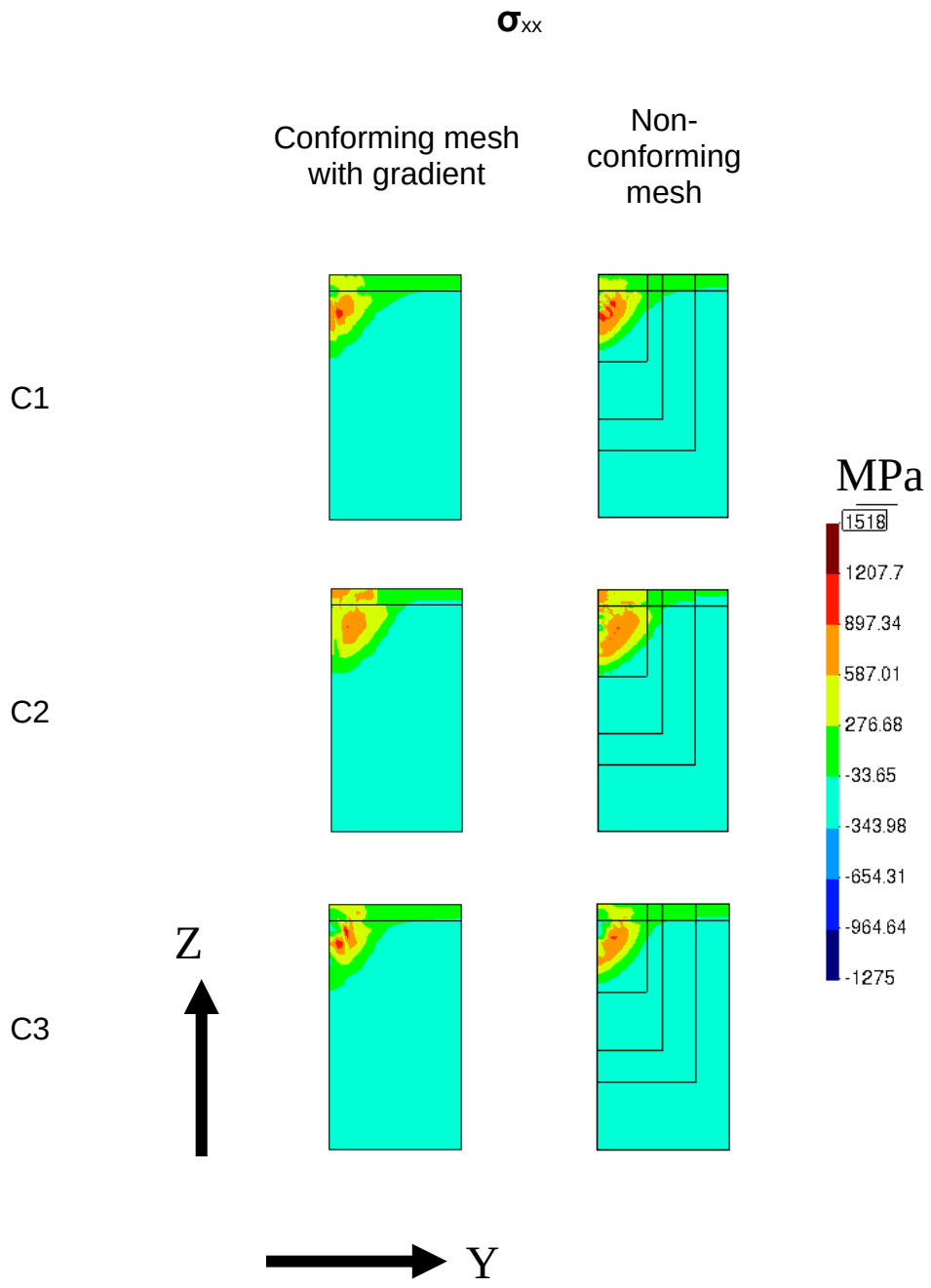

Figure 20: *Stress XX distribution for different cross sections after 0.0075 seconds cooling.*

In the Figure 21, appears the σ_{yy} stresses predicted by each mesh after cooling time. The maximum stress is compressive (-1766 MP) appearing only in the conforming mesh (Figure 21 a)) in the upper part between the powder and the baseplate, in two different specific points. In this case, there is a bigger difference in the Figure 22, around 25%.

The distribution is very similar in both meshes (conforming mesh with gradient and non-conforming mesh) in Figure 21. As in the other cases, the maximum stress is given at the start point of the laser. And these stresses are around 880 MPa.

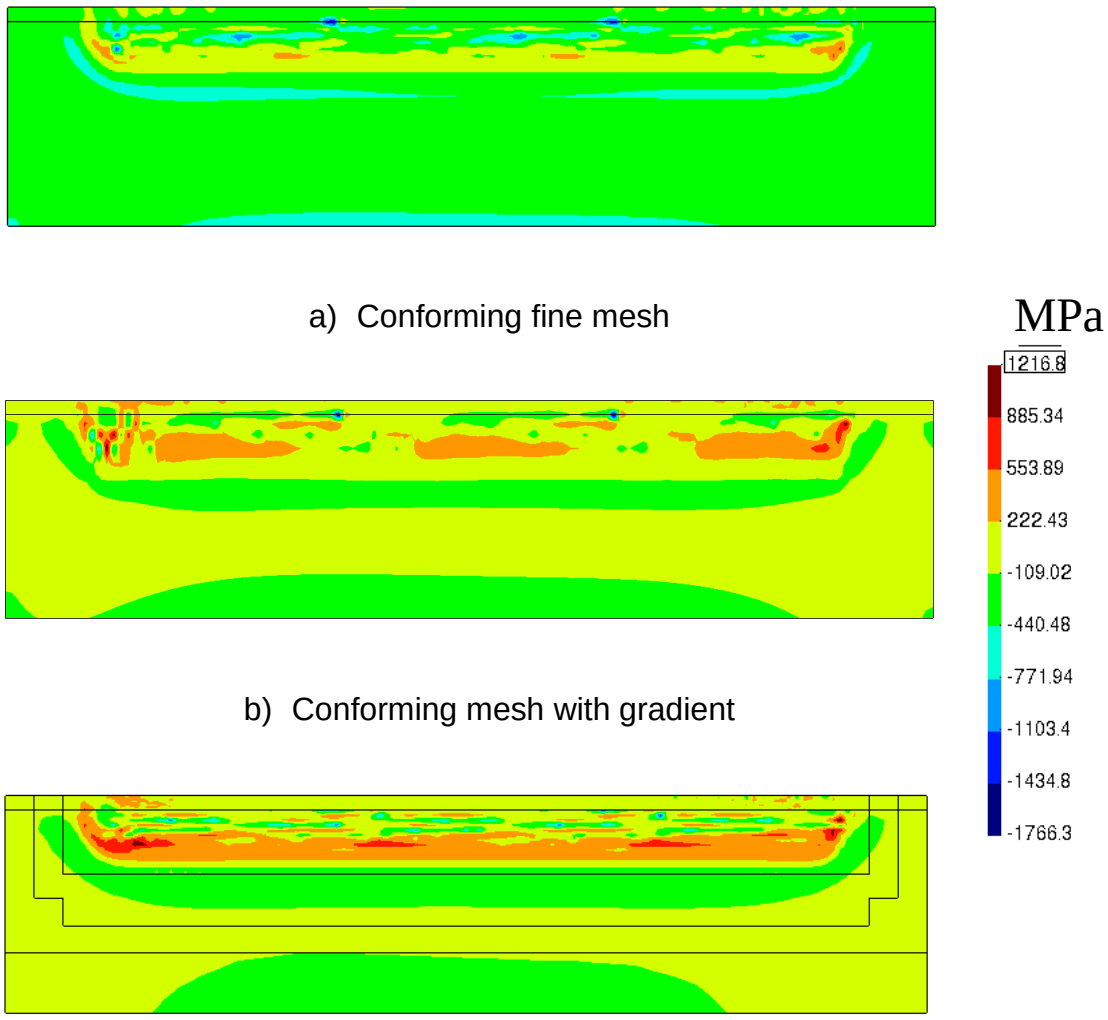

a) Conforming fine mesh

b) Conforming mesh with gradient

c) Non-conforming mesh

Figure 21: *Distribution of the predicted stress YY after 0.0075 seconds cooling.*

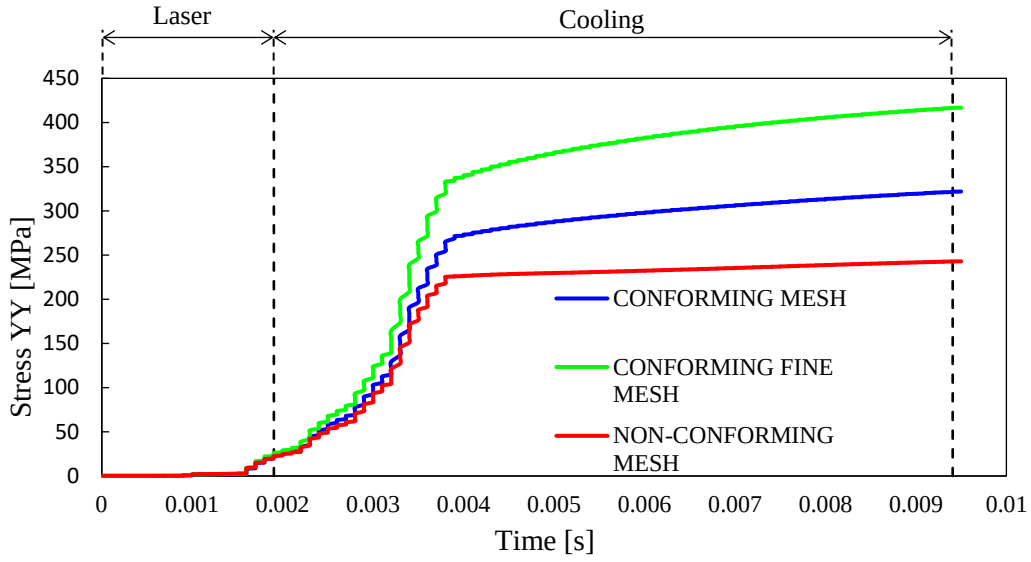

Figure 22: *Predicted stress YY evolution in the middle point of the laser track, comparing both types of meshes.*

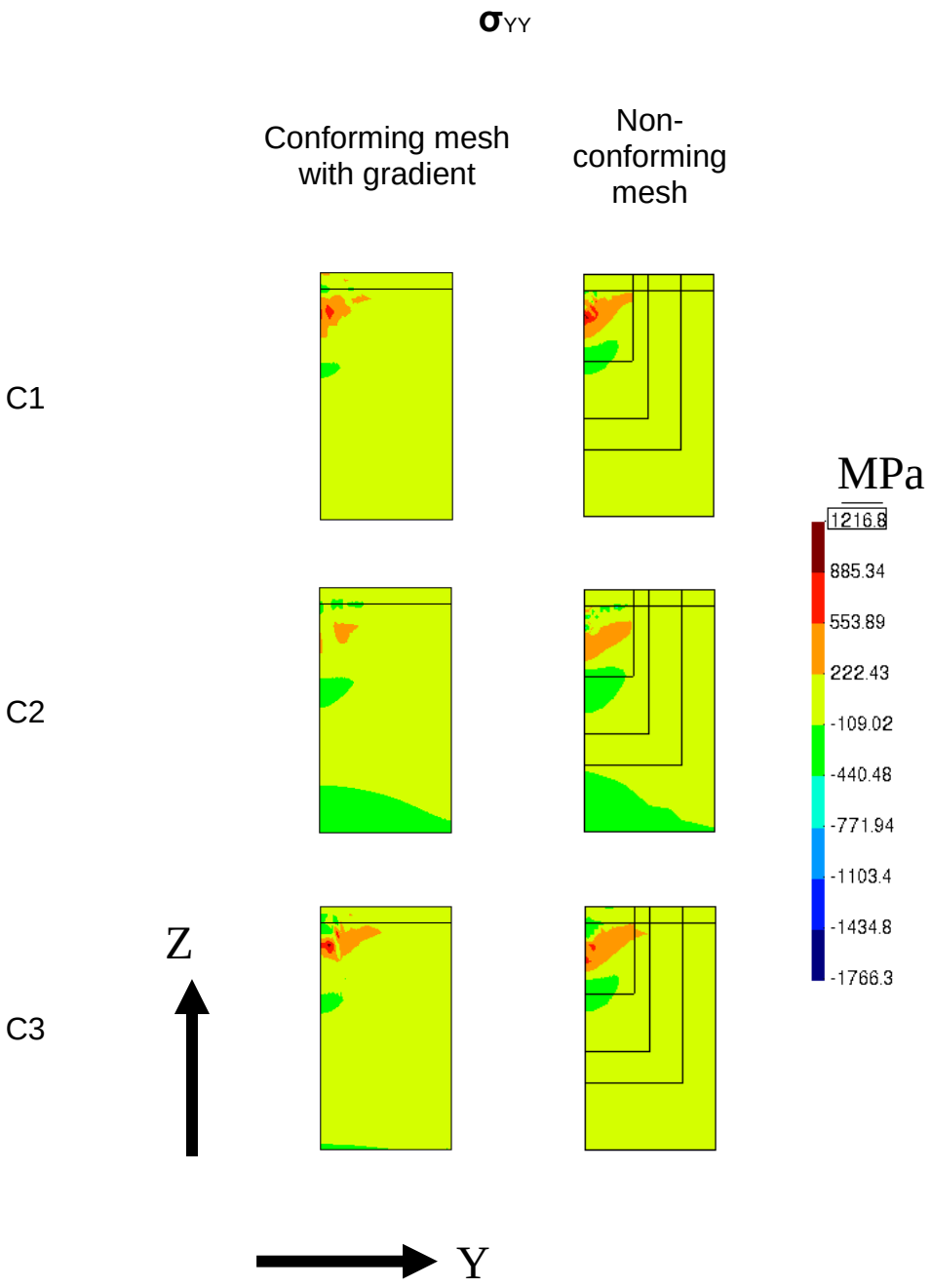

Figure 23: *Stress YY distribution for different cross sections after 0.0075 seconds cooling.*

Figure 24 represents the σ_{zz} in the point of the Figure 8. The maximum stress is compressive around -1800MPa and is given in the conforming mesh. In the same two points as mentioned before in Figure 21. The difference between the meshes

is very similar to the Figure 21, 25%. And like in the other cases these difference starts in the same point.

Figure 22: *Predicted stress YY evolution in the middle point of the laser track, comparing both types of meshes.*

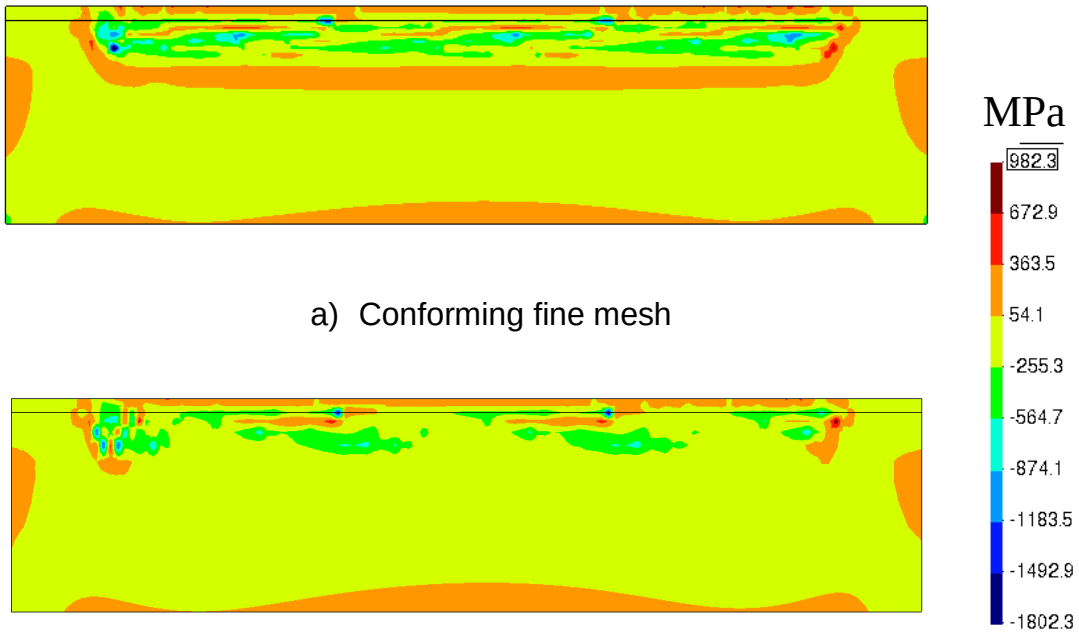

a) Conforming fine mesh

b) Conforming mesh with gradient

c) Non-conforming mesh

Figure 24: *Distribution of the predicted stress ZZ after 0.0075 seconds cooling.*

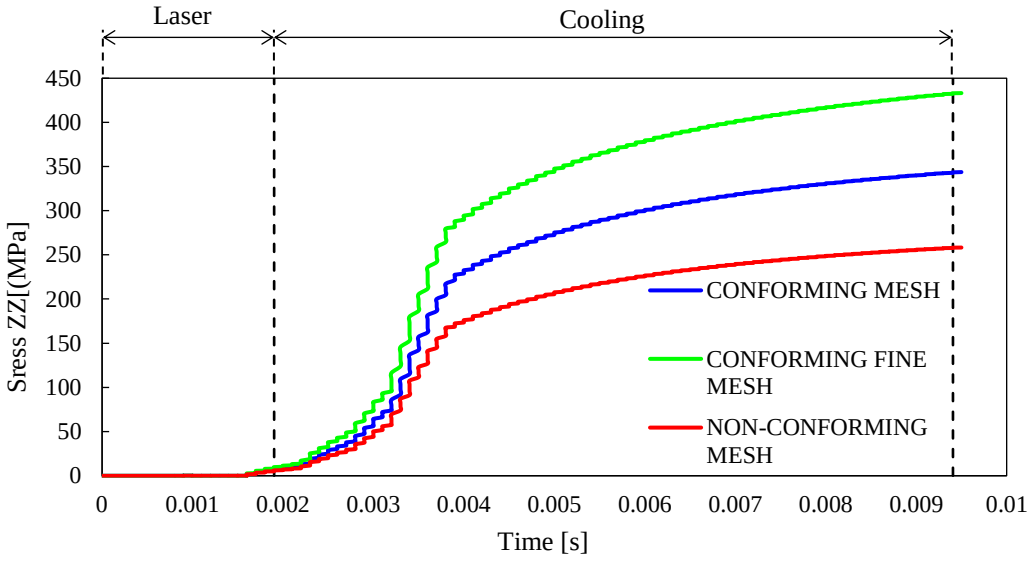

Figure 25: *Predicted stress ZZ evolution in the middle point of the laser track, comparing both types of meshes.*

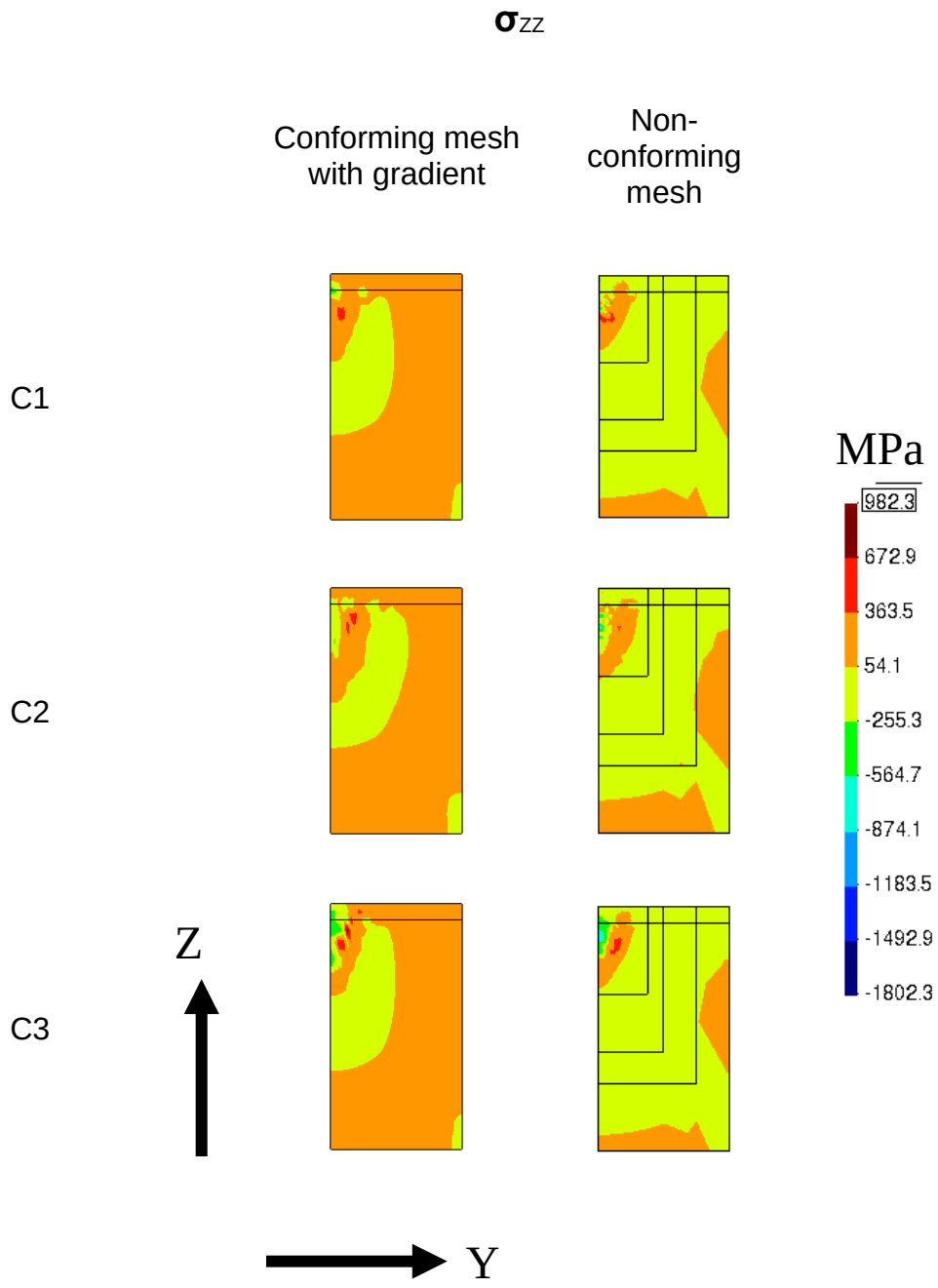

Figure 26: *Stress ZZ distribution for different cross sections after 0.0075 second cooling.*

5. ECONOMICAL REPORT

This section presented the costs of this project. Firstly, the personnel cost is presented (see Table 12). In this case, only the student's time has been considered.

Table 12: *Personnel cost of the economical report.*

PERSONNEL COST					
Name	Job	Cost/hour	Hours	Project task	Cost
Adrian Alamo	Industrial engineering Master Student	4.43 €	1,400	Project author	6,202.00 €
TOTAL					**6,202.00 €**

Secondly, the software used to develop the project are presented. These costs were searched so they are not real values, they are approximations made by the student (see Table 13).

Table 13: *Software cost of the economical report.*

SOFTWARE COST		
Program	Description	Cost
Microsoft office	Microsoft office licence for the development of the project	310.66 €
Mendely Desktop	Mendeley Desktop license for the development of the project	Free
GID	GID license for the pre and post processing of the simulations	540.00 €
DD3IMP	DD3IMP license for running the simulations	Unknown
SUBTOTAL		850.66 €
IVA 21%		
TOTAL		**1,029.3 €**

Thirdly, the cost of the computer used for this project are specified. The costs that they appear in Table 14 are estimations.

Table 14: *Computer cost of the economical report.*

COMPUTER COST	
Intel® Core™ i7-2600K 3.40GHz 8GB RAM	679.00 €
Intel® Core™ i7-4770K 3.50GHz 16GB RAM	800.00 €
TOTAL	**1,479.00 €**

To summarize, the total cost of the project has been taken into account and the total cost of the project has been calculated in the next Table 15.

Table 15: *Project total cost.*

PROJECT TOTAL COST	
Personnel cost	6,202.00 €
Software cost	1,029.3 €
Computer cost	1,479.00 €
PROJECT TOTAL	**8,710.3 €**

6. ENVIROMENTAL AND SOCIAL IMPACT

Numerous studies confirm that 2019 saw the highest temperatures of all time, making it the hottest decade on record. Greenhouse gases increased to record levels in 2019. Climate change is affecting all countries and it is everyone's responsibility to reduce the amount of greenhouse gases. Urgent action is needed to tackle this climate emergency. And this is where industrial engineers have a great responsibility and where they can really make a difference.

When an engineer is carrying out a project, it is mostly based on cost reduction. This is because the market is becoming more and more competitive, and we all do our best to this end. However, it is a mistake to focus mainly on cost reduction without considering the climate impact of what we are developing. Specifically, goal 13 of the SDGs (Climate Action) is the most focused on taking urgent action to combat climate change and its effects.

We also have a major impact on SDG 12 (Sustainable Consumption and Production). This SDG seeks to promote the sustainable management and efficient use of natural resources, as well as to reduce waste generation. Regarding to this goal, when carrying out a project, we should not only focus on cost reduction as mentioned above, but also on the life span of the product we are developing, its recyclability and the natural resources we are going to use to manufacture it.

This is where this project can improve society and considerably reduce material consumption. With this technology, material waste can be reduced considerably. It also greatly reduces stock and the need to manufacture moulds. In addition, it facilitates localised production offering less dependence on suppliers and savings in terms of transport and inventory costs.

Currently, the biggest environmental impact of additive manufacturing, more specifically in the SLM process, is generated in the energy used to produce a laser with sufficient energy to melt the metal. And this is where a real challenge related to consumption arises. Achieving more efficient ways of producing this

laser will have a direct impact on energy consumption and thus a lower environmental impact.

Goal 7 of the SDGs (Affordable and clean energy) refers to ensuring access to affordable, secure, sustainable and modern energy. Given that the SLM process consumes a high amount of energy, it is a very interesting point to look at where the energy it consumes comes from. In this way, contracts could be made with electricity companies to ensure that the energy we consume comes from renewable or low CO2 emission resources, as nowadays it is impossible to supply all the energy consumed with renewable energy.

7. CONCLUSIONS

Starting with the main objective of the project that is the numerical modelling of the SLM process using the finite element method and to reduce the computational cost of simulations in SLM processes by optimizing and characterizing the meshes, the following conclusions have been extracted:

It is important to analyse the thermal model first, as the simulations are much faster and the changes in the mesh, they can do it faster. Once the model is fully defined, the thermo mechanical simulation can be performed, which are significantly slower due to the strong increase of degrees of freedom.

Typically, the non-conforming meshes require less computational time that the conforming meshes since an efficient distribution of the elements in attained. On the other hand, they provide accurate results for the temperature and stress distribution. Since, the important area to analyse is the upper part, the non-conforming mesh allows to concentrate more the elements and nodes in this area thus achieving more accuracy.

Before analysing a non-conforming mesh is important to do it first a thermal simulation with a big conforming mesh in order to have a first results and to have an idea what dimensions it is going to have the melt pool area. After doing this first thermal simulation that is not going to have a very big computational cost, and once that the melt pool area is measured, it can be defined in which area of the mesh the smallest elements will be placed in order to achieve the highest precision and the lowest computational cost.

For the thermal model both meshes provide similar results but for the thermo-mechanical analysis the non-conforming mesh is more accurate. This is because the most impact for the stresses is in the lowest part of the melt pool and in this area the non-conforming mesh have more elements that the conforming mesh.

8. FUTURE LINES

The AM industry is growing and is therefore in a state of continuous improvement, which is why there is still a lot of room for improvement. Nevertheless, this project has been focused on the numerical modelling of the SLM process using finite element method and trying to reduce the computational cost. Because of these, the future lines of this section will be focused in these problems. Many aspects can be improved in a close future for every project developed, continuous improvement is key in engineering. In this section appears the ideas that can be implemented in the future.

First, one of the cases in this study because the results are so different in some cases are the poor data in the Yield stress. For future simulations, in order to have more accurate results it would be a good idea to increase these data.

Also, it would be interesting to extend the study to other materials (high resistance aluminium alloys, titanium alloys, etc.) as well as different laser parameters or other deposition strategies.

As it is mentioned in the study, other factor to take into account it would be to do different analysis in the micro (melt-flow dynamics, discrete element modelling of the powder, etc.), meso and macro scales modelling.

In this study, only a unique non-conforming mesh has been studied. Different types of non-conforming meshes can be studied in order to reduce the computational cost and to obtain more accurate results.

9. PERSONAL ASSESSMENT

The realization of the internship in a foreign country and the Master´s final degree project provides different knowledge that cannot be acquired in your country. In my specific case, working for the University of Coimbra has contributed to understanding the methods used in the research. During the project I have encountered challenges that overcoming them has given me the opportunity to the self-teaching besides learning on my own to solve these problems.

First of all, I would like to thank Dr. Diogo Neto for his big effort and his interest in developing a rich project; his main objective has been my academic development. He is an expert in mechanical engineering from Universidade de Coimbra. We worked for these 7 months together from the early beginning. His experience and expertise have been helpful. He was always able when I needed, and he always took the time necessary for me to understand everything.

What I learned previously in the master`s degree has been of great help to me when working on this project, as several of the knowledge acquired in these six years of the university, such as finite element method (FEM), thermal and mechanical problems, 3D design programs (SolidWorks), etc., has been very useful.

Moreover, in Universidade de Coimbra I could learn how to use two new programs (GID and DD3IMP). Also, how it works the selective laser melting and expand my knowledge in the term of additive manufacturing.

The practices have been very satisfying in all academical, social and self-fulfilment aspects. I am grateful that I can learn and share ideas in the Universidade de Coimbra with selective laser melting technology. This year has not been easy due to COVID-19, a lot of time of the internship I must worked in my house caused by the mobility restrictions in Portugal. In any case, I recommend coming abroad for an internship in the city of Coimbra. Is the city of the students in Portugal and there are people from all the countries and cultures. I can say that I have grown both academically and personally the fact of meeting

so many people give you the addition of the languages, academically speaking but also of understanding of other cultures and be more open minded.

This research work was sponsored by national funds from the Portuguese Foundation for Science and Technology (FCT) under the project with reference PTDC/EME-EME/31657/2017 and by European Regional Development Fund (ERDF) through the Portugal 2020 program and the Centro 2020 Regional Operational Programme (CENTRO-01-0145-FEDER-031657).

10. BIBLIOGRAPHY

[1] K. Solberg, “Doctoral thesis Fatigue design for metallic components produced by additive,” 2021.

[2] S. Singh, S. Ramakrishna, and R. Singh, “Material issues in additive manufacturing: A review,” *J. Manuf. Process.*, vol. 25, no. August 2018, pp. 185–200, 2017, doi: 10.1016/j.jmapro.2016.11.006.

[3] A. L. Maider, “Research in metal additive manufacturing by wire and arc (WAAM).,” *Mondragon Unibertsitatea*, 2019.

[4] T. DebRoy *et al.*, “Additive manufacturing of metallic components – Process, structure and properties,” *Prog. Mater. Sci.*, vol. 92, pp. 112–224, 2018, doi: 10.1016/j.pmatsci.2017.10.001.

[5] N. Roussel, J. Spangenberg, J. Wallevik, and R. Wolfs, “Cement and Concrete Research Numerical simulations of concrete processing : From standard formative casting to additive manufacturing,” *Cem. Concr. Res.*, vol. 135, no. June, p. 106075, 2020, doi: 10.1016/j.cemconres.2020.106075.

[6] L. A. Parry, “Investigation of Residual Stresses,” *Univ. Nottingham*, 2017, doi: 10.4028/www.scientific.net/KEM.627.129.

[7] M. B. Arrillaga and I. Taha, “A review of additive manufacturing technologies and markets for thermosetting resins and their potential for carbon fiber integration,” *Addit. Manuf.*, vol. 37, no. December 2020, p. 101748, 2021, doi: 10.1016/j.addma.2020.101748.

[8] T. Vaneker, A. Bernard, G. Moroni, I. Gibson, and Y. Zhang, “CIRP Annals - Manufacturing Technology Design for additive manufacturing : Framework and methodology,” vol. 69, pp. 578–599, 2020, doi: 10.1016/j.cirp.2020.05.006.

[9] F. Le, B. Olivier, and J. H. P. Mognol, “Sustainable manufacturing :

evaluation and modeling of environmental impacts in additive manufacturing," pp. 1927–1939, 2013, doi: 10.1007/s00170-013-5151-2.

[10] S. H. Huang, P. Liu, and A. Mokasdar, "Additive manufacturing and its societal impact : a literature review," pp. 1191–1203, 2013, doi: 10.1007/s00170-012-4558-5.

[11] J. Faludi, C. Bayley, S. Bhogal, and M. Iribarne, "Comparing environmental impacts of additive manufacturing vs traditional machining via life-cycle assessment," vol. 1, no. October 2013, pp. 14–33, 2015, doi: 10.1108/RPJ-07-2013-0067.

[12] 3DEO, "Environmental Impact of Additive Manufacturing." https://news.3deo.co/environmental-impact-of-additive-manufacturing.

[13] F. Matos, R. Godina, C. Jacinto, and H. Carvalho, "Additive Manufacturing : Exploring the Social Changes and Impacts," 2019.

[14] E. L. Papazoglou, N. E. Karkalos, P. Karmiris, and A. P. Markopoulos, *On the Modeling and Simulation of SLM and SLS for Metal and Polymer Powders : A Review*, no. 0123456789. Springer Netherlands, 2021.

[15] B. K. Nagesha, S. A. Kumar, K. Vinodh, A. Pathania, and S. Barad, "Materials Today : Proceedings A thermo – Mechanical modelling approach on the residual stress prediction of SLM processed HPNGV aeroengine part," *Mater. Today Proc.*, vol. 44, pp. 4990–4996, 2021, doi: 10.1016/j.matpr.2020.12.940.

[16] H. Tran and Y. Lo, "Heat transfer simulations of selective laser melting process based on volumetric heat source with powder size consideration," *J. Mater. Process. Tech.*, vol. 255, no. May 2017, pp. 411–425, 2018, doi: 10.1016/j.jmatprotec.2017.12.024.

[17] C. Methods, A. Mech, Y. Zhang, G. Guillemot, M. Bernacki, and M. Bellet, "ScienceDirect Macroscopic thermal finite element modeling of additive metal manufacturing by selective laser melting process," *Comput. Methods*

Appl. Mech. Engrg., vol. 331, pp. 514–535, 2018, doi: 10.1016/j.cma.2017.12.003.

[18] M. Markl and K. Carolin, “Multiscale Modeling of Powder Bed – Based Additive Manufacturing,” doi: 10.1146/annurev-matsci-070115-032158.

[19] L. Bertini, F. Bucchi, F. Frendo, M. Moda, and B. Disma, “A critical review of simulation strategies,” pp. 609–636, 2019.

[20] J. M. P. Martins, J. L. Alves, D. M. Neto, M. C. Oliveira, and L. F. Menezes, “Numerical analysis of different heating systems for warm sheet metal forming,” *Int. J. Adv. Manuf. Technol.*, vol. 83, no. 5–8, pp. 897–909, 2016, doi: 10.1007/s00170-015-7618-9.

[21] B. M. Marques, C. M. Andrade, D. M. Neto, M. C. Oliveira, J. L. Alves, and L. F. Menezes, “Numerical Analysis of Residual Stresses in Parts Produced by Selective Laser Melting Process,” *Procedia Manuf.*, vol. 47, no. 2019, pp. 1170–1177, 2020, doi: 10.1016/j.promfg.2020.04.167.

[22] J. M. P. Martins *et al.*, “International Journal of Solids and Structures A new staggered algorithm for thermomechanical coupled problems,” *Elsevier*, vol. 123, pp. 42–58, 2017, doi: 10.1016/j.ijsolstr.2017.06.002.

[23] C. Methods, A. Mech, S. H. Huo, G. R. Liu, J. Q. Zhang, and C. M. Song, “A smoothed finite element method for octree-based polyhedral meshes with large number of hanging nodes and irregular elements,” *Comput. Methods Appl. Mech. Eng.*, vol. 359, p. 112646, 2020, doi: 10.1016/j.cma.2019.112646.

[24] M. J. B. J.M. MCDILL, J. A. GOLDAK, A. S. ODDY, “ISOPARAMETRIC QUADRILATERALS AND HEXAHEDRONS FOR MESH-GRADING ALGORITHMS,” *Carlet. Univ.*, vol. 3, no. September 1986, pp. 155–163, 1987.

[25] A. H. Elsheikh and M. Elsheikh, “Advances in Engineering Software A consistent octree hanging node elimination algorithm for hexahedral mesh

generation," *Adv. Eng. Softw.*, vol. 75, pp. 86–100, 2014, doi: 10.1016/j.advengsoft.2014.05.005.

[26] T. Fries, A. Byfut, A. Alizada, and K. W. Cheng, "Hanging nodes and XFEM," no. September 2010, pp. 404–430, 2011, doi: 10.1002/nme.

[27] K. Saurabh, B. Gao, M. Fernando, S. Xu, and M. A. Khanwale, "Industrial scale Large Eddy Simulations with adaptive octree meshes using immersogeometric analysis," *Comput. Math. with Appl.*, vol. 97, no. February, pp. 28–44, 2021, doi: 10.1016/j.camwa.2021.05.028.

[28] M. Carraturoa, S. Kollmannsbergerb, A. Realia, F. Auricchioa, and E. Rankc, "An immersed boundary approach for residual stress evaluation in SLM processes."